SYNTHESIS OF INDANDIONE-BASED POROUS ORGANIC POLYMERS AND THEIR APPLICATIONS IN ZINC-ION BATTERIES

A Thesis Submitted to
the Graduate School of Engineering and Sciences of
İzmir Institute of Technology
in Partial Fulfillment of the Requirements for the Degree of

MASTER OF SCIENCE

in Chemistry

by

Gizem ŞİMŞEK

December 2022
İZMİR

ACKNOWLEDGMENTS

I would like to thank everyone for their help, support, and guidance during my two-year graduate education. I want to like to express my gratitude to Dr. Onur Büyükçakır, who provided me the opportunity to work in his research laboratory, and for his patience, guidance, support, and motivation in both science and life. It has been a great honor for me to work with him.

I would like to thank The Scientific and Technological Research Council of Türkiye for its financial support for this project. (220Z024)

I would like to thank my first laboratory friend, Ferit Begar, and all Büyükçakır Research Group members Yaren Naz Erözen, Mustafa Erdoğmuş, Utku Cem Çanakçı, Yasmin Geçalp and Hüseyin Zeybek for their endless help and friendship during my studies.

I am very thankful to committee members, Prof. Dr. Levent Artok and Prof. Dr. Derya Gülcemal, for their precious time and support.

I would like to thank my dear mother Neriman Şimşek, who encouraged and supported me throughout my education life, my father Erdoğan Şimşek, my dear sister Ezgi Yağmur Şimşek Demirci and Serkan Demirci.

I would like to thank especially Merve Tufaner and Esra Güleç, as well as Sevcan Mert, Esra Filiz, Buğra Güngül, Cansın Esringü, Hazal Özsoy, Mert Akçalı, Anıl Dağlı, for their friendship, who stood by me whenever I needed them.

Lastly, I would like to thank Cafer Özdamar, the most special person in my life, who stood by me every time I fell, for his support and unconditional love.

ABSTRACT

SYNTHESIS OF INDANDIONE-BASED POROUS ORGANIC POLYMERS AND THEIR APPLICATIONS IN ZINC-ION BATTERIES

There has been growing interest in porous organic polymers (POPs) in recent years due to their large surface area, easy chemical tunability, sustainability, and high thermal and chemical stability. Due to their exceptional properties, they are suitable for use as platforms in various applications, including gas storage, separation, catalysis, and, more recently, energy storage systems. In this regard, it is imperative to design new functional POPs with a large surface area, permanent porosity, and physicochemical stability.

In this thesis, we have presented indandione-based POPs (r-POPs) prepared by an acid-catalyzed condensation reaction between s-indacene-1,3,5,7(2H,6H)-tetraone and benzene-1,3,5-tricarboxaldehyde under highly environmentally friendly conditions. In order to optimize the reaction conditions, we first synthesized the model compound, namely 2-benzylidene-1H-indene-1,3(2H)-dione. The model compound was characterized by using ^{1}H and ^{13}C-NMR spectroscopy. Using different types of acids, we have investigated the effect of acid on polymerization and its textural properties. The polymers were characterized using various characterization techniques. Due to increased interest in renewable energy as a fossil fuel substitute, energy storage systems have attracted colossal interest, and rechargeable aqueous zinc-ion batteries (ZIBs) are seen as promising energy storage systems, particularly for grid-scale applications. In this respect, the carbonyl-rich structure of r-POPs transforms them into a potential electrode material. Thus, we have also investigated their electrochemical performances as cathode materials for ZIBs. Although r-POPs showed low electrochemical performance in capacity and cycle life, they have great potential to be an electrode material in other metal-ion batteries.

ÖZET

İNDANDİON BAZLI GÖZENEKLİ ORGANİK POLİMERLERİN SENTEZİ VE ÇİNKO-İYON PİLLERDEKİ UYGULAMALARI

Son yıllarda, geniş yüzey alanları, kolay kimyasal ayarlanabilirlikleri, sürdürülebilirlikleri ve yüksek termal ve kimyasal kararlılıkları nedeniyle gözenekli organik polimerlere (GOP'lar) artan bir ilgi var. İstisnai özellikleri nedeniyle, gaz depolama, ayırma, kataliz ve daha yakın zamanda enerji depolama sistemleri dahil olmak üzere çok çeşitli uygulamalarda platformlar olarak kullanılmaya uygundurlar. Bu nedenle, geniş bir yüzey alanına, kalıcı gözenekliliğe ve yüksek düzeyde fizikokimyasal stabiliteye sahip yeni fonksiyonel GOP'lar tasarlamak çok önemlidir.

Bu tezde, s-indasen-1,3,5,7(2H,6H)-tetraon ve benzen-1,3,5-trikarboksialdehit arasında son derece çevre dostu koşullarda asit katalizli bir yoğuşma reaksiyonuyla hazırlanan indandion bazlı GOP'ları (r-GOP'lar) sunduk. Reaksiyon koşullarını optimize etmek için önce model bileşiği, 2-benziliden-1H-inden-1,3(2H)-dion'u sentezledik. Model bileşik, ^{1}H ve ^{13}C-NMR spektroskopisi kullanılarak karakterize edildi. Farklı asit türleri kullanarak, asidin polimerizasyon ve dokusal özellikleri üzerindeki etkisini araştırdık. Polimerler, çeşitli karakterizasyon teknikleri kullanılarak karakterize edildi. Fosil, yakıt ikamesi olarak yenilenebilir enerjiye olan ilginin artması nedeniyle, enerji depolama sistemleri muazzam bir ilgi gördü ve şarj edilebilir sulu çinko-iyon piller (ZIB'ler), özellikle şebeke ölçekli uygulamalar için umut verici enerji depolama sistemleri olarak görülüyor. Bu açıdan, r-GOP'ların karbonil açısından zengin yapıları onları potansiyel bir elektrot malzemesine dönüştürür. Bu sebeple, ZIB'ler için katot malzemeleri olarak elektrokimyasal performanslarını da araştırdık. r-GOP'lar, kapasite ve çevrim ömrü açısından düşük elektrokimyasal performans gösterseler de, diğer metal-iyon pil türlerinde bir elektrot malzemesi olma potansiyelleri yüksektir.

TABLE OF CONTENTS

LIST OF FIGURES

Figure **Page**

Figure **Page**

ABBREVIATIONS

^{1}H	Proton Nuclear Magnetic Resonance Spectroscopy
CV	Cyclic Voltammetry
^{13}C	Carbon Nuclear Magnetic Resonance Spectroscopy
FTIR	Fourier- Transform Infrared Spectroscopy
$KMnO_4$	Potassium permanganate
NMP	N-methyl-2-pyrrolidone
NMR	Nuclear Magnetic Resonance
SEM	Scanning Electron Microscopy
TGA	Thermogravimetric Analysis
XRD	X-ray Diffraction Analysis
EtOH	Ethanol
EtOAc	Ethyl Acetate
CH_3CN	Acetonitrile
BET	Brunauer-Emmett-Teller
MeOH	Methanol
$CDCl_3$	Deuterated chloroform
IUPAC	International Union of Pure and Applied Chemistry
DCM	Dichloromethane
DMSO	Dimethyl sulfoxide
THF	Tetrahydrofuran
s	Singlet
d	Doublet
t	Triplet
m	Muttiplet
dd	Doublet of Doublet

CHAPTER 1

INTRODUCTION

1.1. An Overview

In recent years, the need for energy has been increasing worldwide. In this respect, using renewable energy sources to meet the increasing energy demand has become the focus of both industry and academic fields. However, the intermittent nature of renewable energy sources makes energy storage systems imperative. In this regard, the development of energy storage systems has attracted significant attention, and many scientific studies have been carried out to develop high-performance energy storage systems. Among energy storage systems, the electrochemical system is the most promising and efficient one, converting chemical energy into electrical energy through electrochemical reactions.[1] Particularly, rechargeable metal-ion batteries have many advantages compared to other electrochemical energy storage systems. It offers high energy density (how much energy it can store in the system) and power density (how long it can transfer the stored energy) with long cycle life.[2] There is no doubt that rechargeable lithium-ion batteries (LIBs) have served society by powering many portable devices and electric vehicles. Even though LIBs have high theoretical capacities and stable energy outputs, their applications are restricted to large-scale energy storage systems and biological uses. This is because lithium metal is inherently flammable, and using flammable electrolytes is unavoidable. Furthermore, lithium resources are in short supply.[3] On the other hand, zinc-ion batteries (ZIBs) have attracted more attention in energy storage in recent years. Among rechargeable metal-ion battery systems, aqueous rechargeable ZIBs are more suitable for large-scale energy storage systems due to their relatively large theoretical specific capacities, high safety, low redox potential (-0.762 V against standard hydrogen electrode), low cost, and nontoxicity. Although ZIBs offer superior features, many challenges must be addressed to develop high-performance aqueous rechargeable ZIBs. Despite the challenges associated with anode and electrolytes, most current studies focus on developing new cathode materials. Up to now, several inorganic-based cathode

materials have been reported. Although manganese and vanadium-based electrode materials showed high specific capacities, they suffer from poor cycle stability and capacity fading with increasing charge-discharge cycles. [4-5] On the other hand, organic cathode materials provide high structural tenability, sustainability, and electrochemical performance. To date, several organic compounds have been tested in aqueous rechargeable ZIBs. However, most of them exhibit poor cycle performance and low capacities because of the high solubility of their discharged products and low electrical conductivity. For this reason, developing new cathode materials bearing high electrochemical performance plays a crucial role in fabricating next-generation aqueous rechargeable ZIBs.

1.2. Porous Organic Polymer (POPs)

Porous structures are abundant in the natural world. Numerous samples of natural solid materials, such as stone, coal, and rock, possess persistent pores. These pores exist in numerous sizes and shapes.[6] Porous organic polymers, also known as POPs, are characterized by the presence of permanent pores that range in both size and shape. Porous materials are classified by the International Union of Pure and Applied Chemistry (IUPAC) into one of three categories based on the size of their pores. In this regard, POPs can be categorized based on the size of the pores that they possess. Microporous polymers have a pore size that is less than 2 nanometers in diameter ($d<2$ nm), as measured in diameter. On the other hand, mesoporous polymers contain mesopores with a pore diameter that ranges between 2 nm to 50 nm. Lastly, macroporous materials are those that have pores that are larger than 50 nanometers in size [7-8] (Figure 1.1)

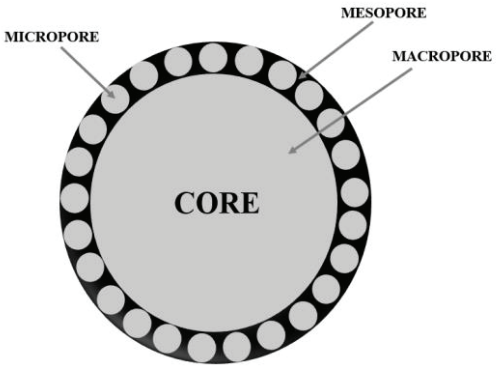

Figure 1.1 Schematic representation of the size of the pores.

POPs can also be categorized based on the synthesis methodologies that were utilized to create them. These polymeric materials include covalent organic frameworks (COFs), hyper-crosslinked polymers (HCPs), covalent triazine frameworks (CTFs), porous aromatic frameworks (PAFs), and conjugated microporous polymers (CMPs). Most POPs are amorphous polymeric networks, even though COFs and CTFs exhibit long-range ordered (crystalline) frameworks. (Figure 1.2) Although these distinct polymers have unique structural characteristics, they may all be manufactured to have a high porosity, contain light components, and have highly covalently bonded two-dimensional or three-dimensional structures.[6]

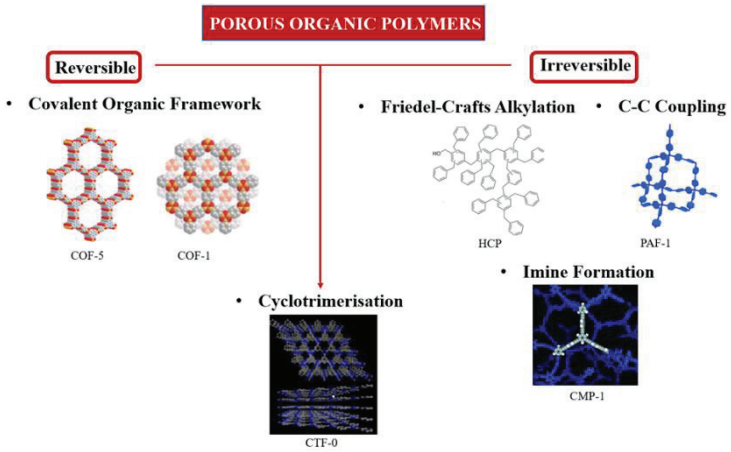

Figure 1.2 Porous polymers: Covalent Organic Frameworks (COFs)[8], Hyper crosslinked Polymers (HCPs)[9], Covalent Triazine Frameworks (CTFs)[10], porous aromatic frameworks (PAFs)[11], and Conjugated Microporous Polymers (CMPs)[12]

1.3 Covalent Organic Frameworks (COFs)

Covalent-organic frameworks (COFs) are often formed from light elements such as H, B, C, N, and O by strong covalent bonds. These polymeric frameworks show, crystallinity with ordered, well-defined porosity.[13] Structural design and the chemistry used to link monomeric units enable to construction of long-range ordered networks. Besides their ordered porous structure, they show high physicochemical stability and superior textural properties, including high surface area and large pore volume. These features make COFs suitable platforms for various applications. Building blocks for synthesizing crystalline covalent-organic frameworks (COFs) must have suitable geometry and proper functional groups that can be linked via reversible reaction pathways that yield thermodynamic products.[14-15] COFs can be synthesized using variable reaction pathways and monomeric building blocks bearing different structures, functional moieties, sizes, and dimensions. Some of the linking groups used in COF structures are shown.(Figure 1.3)

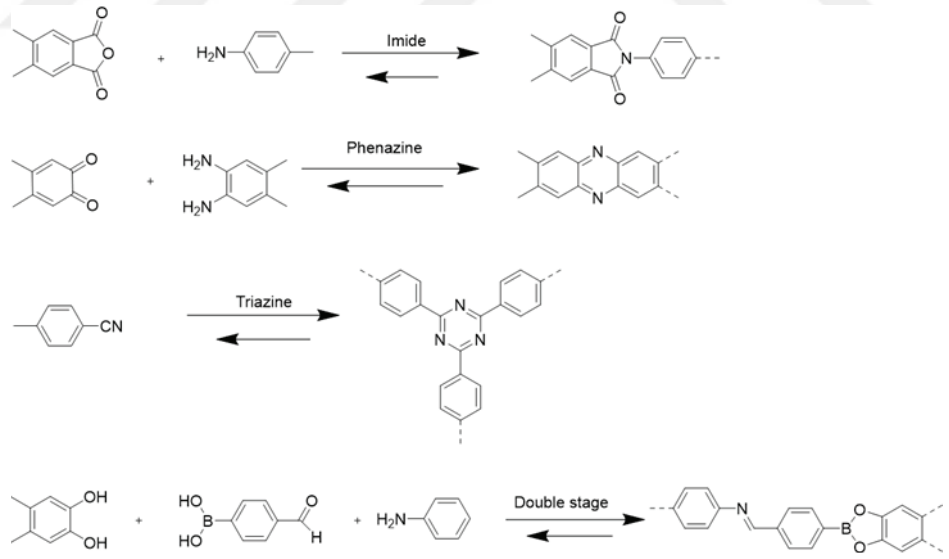

Figure 1.3 Some linking units used in COF structures.

COF structures are porous polymeric materials, and most have planarly arranged 2D layers with the help of large conjugated aromatic monomers. Layers of organic units are built up from secondary bonds, such as π-π interactions, in 2-dimensional crystalline

COF structures. They can be found in two different configurations: planar growth, a two-dimensional organization with interactions, overlapping AA (eclipsed) stacking, and slipping AB (staggered) stacking[16].(Figure 1.4) Compared to 2D-COF structures, limited examples of 3D-COFs were also reported. Thanks to the geometry of the tetra(4-dihydroxyborylphenyl) TBPM tetrahedral compound, a 3D COF was synthesized by Yaghi and co-workers.[14]

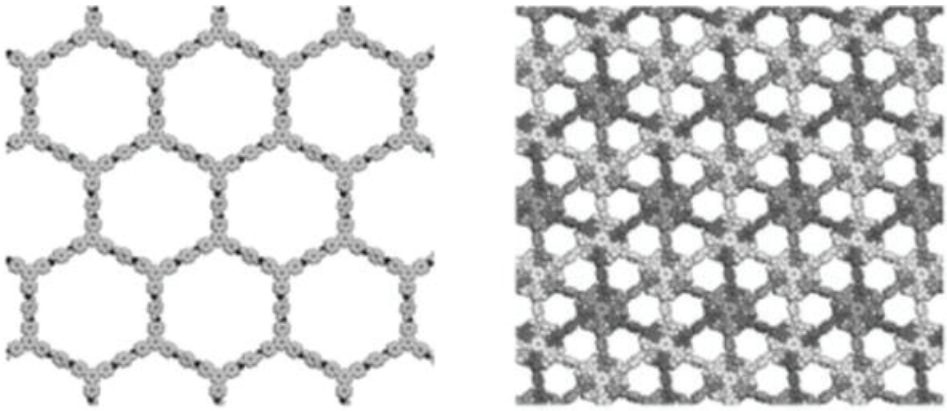

Figure 1.4 Types of stacking seen in Hexagonal and Tetragonal 2D COFs.[16]

Although several different reaction methodologies were used to fabricate COFs, three main synthesis routes were used to create COFs: solvothermal, ionothermal and microwave.

Solvothermal Synthesis

The majority of the COF structures that were described in the literature were synthesized using a solvothermal synthesis approach. This method is also utilized in the production of zeolites.[15] Solvents and reactants used in COF synthesis are kept in a steel autoclave in an oven at 80-150 °C for 3 to 12 days using the solvothermal synthesis method. The pressure created in the autoclave is critical for this synthesis technique. Yaghi and his colleagues discovered that the ideal pressure in the autoclave is 150 mTorr as a consequence of their research. The solvent employed in COF synthesis is critical.[14] To create an optimal COF, a single solvent or a blend of solvents might be utilized. It is

critical that the solvent can dissolve the reactants. The solvent also influences the crystallinity of the COF structure. Using this process, it is possible to obtain amorphous or microcrystalline polymers according to the reaction parameters, such as solvent, temperature, catalyst, and concentration. Despite these synthetic challenges, using different reaction strategies make it possible to synthesize COFs.[17-18-19]

Ionothermal Synthesis

High-quality COFs can also be synthesized using the ionothermal synthesis approach. By cyclotrimerization of 1,4-dicyanobenzene and 2,6 naphthalenedicarbonitrile, which are ditopic monomers, in molten $ZnCl_2$ at 400°C, they formed covalent triazine-based frameworks (CTF) with high crystallinity and thermal strength. Molten $ZnCl_2$ is essential for CTF formations as it acts as a solvent and a catalyst. However, the ionothermal approach is more disadvantageous than the solvothermal method due to the problematic synthesis conditions and exceptionally high-temperature requirements limiting monomers' usage due to decomposition.[20] Furthermore, high temperatures and long reaction times require unavoidable carbonization during the polymerization.

Microwave synthesis

Microwave synthesis is the approach of choice for accelerating the reaction and is used in many areas to get the desired materials within a short time. The process of microwave synthesis can also accomplish the creation of COF structures. Dichtel and co-workers were able to manufacture 2D COF-5 in twenty minutes by making use of reactants, including 2,3,6,7,10,11-hexahydroxytriphenylene and 1.4-benzeneboronic acid.[21-22]

1.4 Potential applications of COFs

COFs can be synthesized with various organic linkers bearing different functional moieties. This versatility in chemical structure enables the usage of COFs in different applications, such as gas storage/separation, catalysis, and energy storage.

1.4.1 Gas Storage

1.4.1.1 Hydrogen Storage

Hydrogen gas is vital for air pollution prevention and as a clean energy source. Its importance as an energy carrier is growing unexpectedly, particularly for transportation applications. Besides conventional carbon-based porous materials, COFs offer high hydrogen uptake performance and superior gas diffusion kinetics.[13] Compared to other porous materials reported in the literature, for example, COF-1 reveals a high hydrogen storage capacity of 1.28 wt%, at 1 bar and 77 K. The high hydrogen uptake values can be attributed to its high BET surface area of 711 $m^2 g^{-1}$, which was calculated from the nitrogen adsorption-desorption isotherms, and its functional skeleton, which enables the optimum interaction with hydrogen gas.[23]

1.4.1.2 Catalysts

Porous materials have long been used as heterogeneous catalysts to catalyze the reaction to get the desired products. Thanks to their large surface areas and high thermal stabilities, zeolites, one of the traditional porous materials, have long been used as catalysts in petroleum chemistry. In this respect, COFs structures have also been used as catalysts because they are naturally porous and can be synthesized with appropriate reactants (functional units) for high surface area. For example, the COF-LZU_1 material

was used as a catalyst in Suzuki-Miyaura coupling reactions, and it was discovered that successful activity was demonstrated as a result of its coordination with $Pd(OAc)_2$.[24]

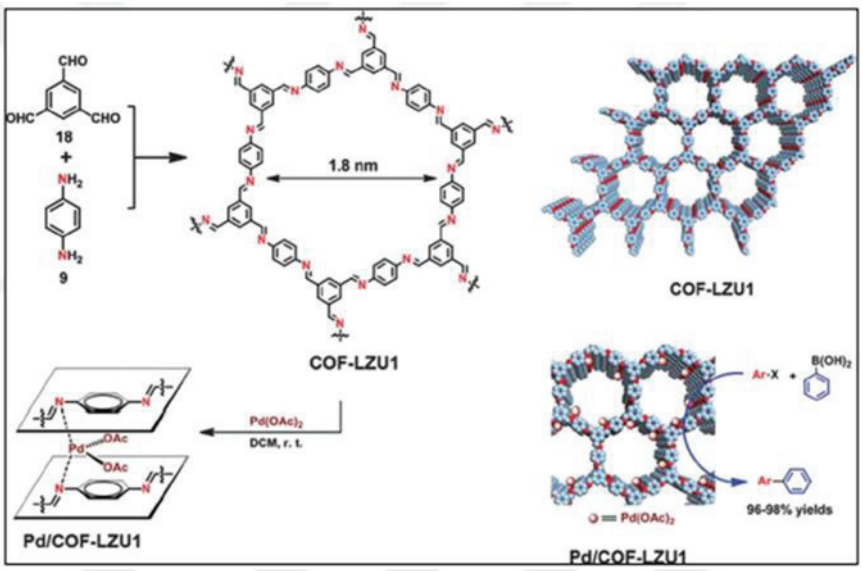

Figure 1.5 Demonstration of the synthesis and working principle of the Pd/COF-LZU_1 compound as a catalyst [24]

1.4.1.3 Carbon Dioxide Storage

The consumption of fossil fuels to meet the energy demand produces a large amount of carbon dioxide (CO_2), known as one of the greenhouse gases, and exacerbates global warming. Because of their low density, high thermal stability, high surface area, and the availability of various synthetic pathways, POPs and its subclasses, i.e. COFs, CTFs, PAFs, HCPs, and CMPs, are considered to be potential candidates for the capture of carbon dioxide (CO_2). Because of their superior features, POPs are of significant interest in CO_2 capture and separation. It has been demonstrated that various POPs can capture carbon dioxide across a wide pressure and temperature range.[61] However, CO_2 uptake capability of POPs is affected by a wide variety of factors, and the ability of POPs to uptake CO_2 can be affected by several factors. There are three primary ways to boost the uptake values. The first one is the increment in surface area and pore volume. Second, the pore surface of polymers should be functionalized with appropriate moieties to generate an optimal environment for CO_2 adsorption by increasing the interaction between CO_2 molecules and the pore surface. Finally, polymers should have optimum

pore size and connected pores to enhance the interaction between pore walls and CO_2 molecules without sacrificing diffusion kinetics.[25] According to reported studies, COF-102, for example, can store up to 1200 mg of carbon dioxide per kilogram at a temperature of 298 K under an atmosphere of 55 bar.[26,27]

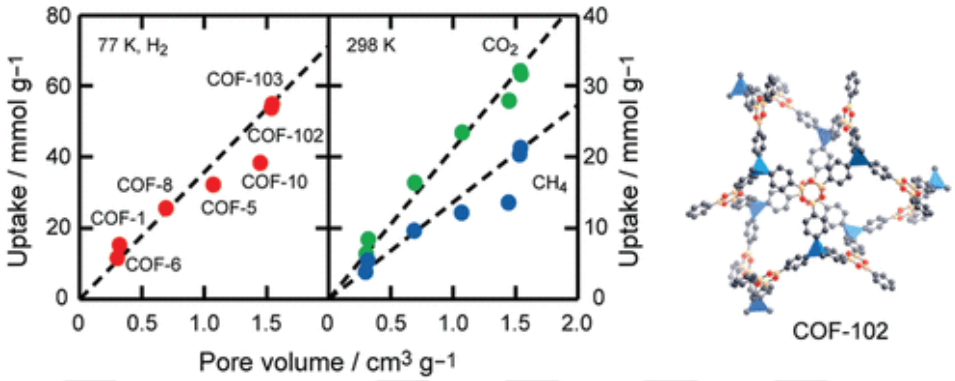

Figure 1.6 Relationship between absolute gas uptake and pore volume of COFs estimated from Ar isotherms. [26]

1.5 Conjugated Microporous Polymers(CMPs)

Conjugated microporous polymers, also known as CMPs for short, are a one-of-a-kind of polymer that are distinguished by their high surface areas, diversity in structure, conjugated polymer structure and linkages, and electron delocalization on the microporous structure.[28] They have been utilized in many areas, including energy storage, gas adsorption, and catalysis.[29-30] However, due to their synthesis prerequisites, most CMPs have been synthesized using heavy metals including catalysts, leading to high cost and environmental problems.[31] Research on polymerization conditions, low-cost monomers, and metal-free synthesis strategies has recently attracted much attention. On the other hand, recently, heavy metal free reactions have been developed to fabricate the CMPs.[32-33] The porous structure of CMPs can be easily manipulated by the design of the monomer units. Furthermore, with the help of rational designs, it is possible to control and tune pore size and surface area of CMPs. Also, the skeleton of CPMs can be functionalized with various functional groups, such as methyl, hydroxyl, carboxyl, and amine moieties, which transform them into desired materials for a specific application.[34,35]

1.6 Redox-Active Porous Organic Polymers for Energy Storage

1.6.1 Working Principle of Batteries

Research into energy storage systems like rechargeable batteries and supercapacitors has risen in popularity to keep up with the proliferation of electronic devices in our society.[36] Altering the structure of redox-active POPs materials can boost their electrochemical performance. To illustrate, nanoscale silica templates of organic building blocks can be modified by including porous redox-active POP materials with thin shell thicknesses. Therefore, hollow POP materials are formed if the silica templates are removed.[37] Thanks to these holes/pores, it can easily be placed on POP materials. As a result, redox-active regions can be used more effectively.[4-37]

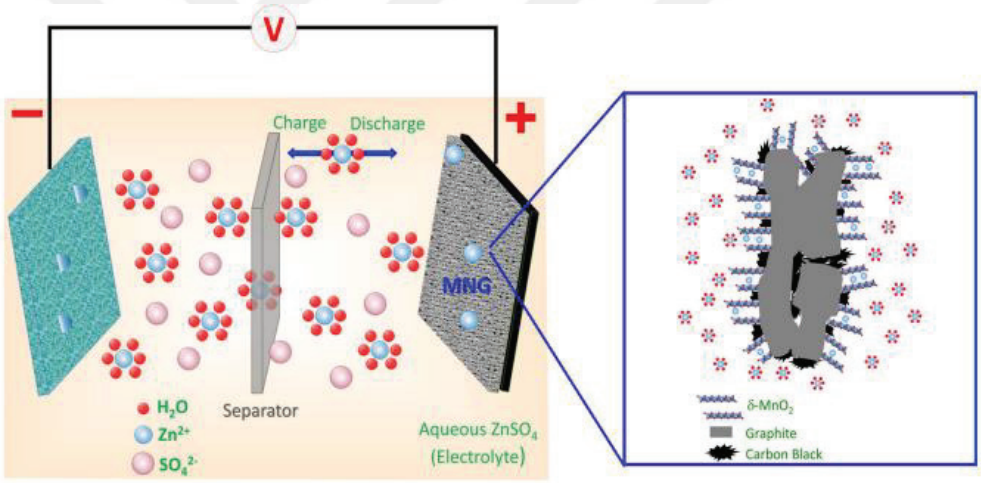

Figure 1.7 Schematic representation of a battery.[38]

The battery consists of four parts: positive electrode (cathode), the negative electrode (anode), separator and electrolyte. These components are the most critical factors that determine the operating performance of a battery. For example, separators play an essential role because if the anode and cathode are in direct contact, the battery will be short-circuited.[39] For zinc-ion batteries, the research mainly focused on the cathode part to design new cathode materials offering high specific capacity and long cycle life with affordable cost. Most of the electrodes, for example, consist of active material, conductors, and binders. The binder keeps the conductor, the active ingredient, and the current carrier all in place. The function of the conductor is to link the conducting

substance with the current carrier and therefore facilitate the flow of electrons. The resistance caused by electron transport can be decreased by ensuring that the active ingredient is uniformly distributed at the reaction site. This dispersion is only possible if the active material makes excellent contact with the conductor. Therefore, several different carbon-based conductors have been used to enhance conductivity and ion/charge transfer kinetics. (Figure 1.7)[38,39]

High energy density, small size, and long cycle life are important features in batteries. The discharge rate is the amount of current drawn from a battery over a period of time. It gives information about the capacity of the battery.[40] Although capacity should be the same as slow discharge in theory, it has been observed that the battery's capacity is higher at a low discharge rate. Capacity is read lower due to internal resistance, potential, and energy losses inside the battery. The same battery can deliver high capacity from even lower discharge currents. The same battery can deliver high capacity from even lower discharge currents. A battery with a discharge rate of 1C does not have good performance. Manufacturers discharge batteries slowly at around 0.05C for 20 hours to obtain an efficient battery. Even at this rate, it is challenging to reach 100% capacity.[41]

1.7 Lithium-ion Batteries

Lithium is the strongest reducing (reduction potential -3.04 V vs. standard hydrogen electrode, SHE) and the lightest (specific gravity p=0.53 g/cm³, molecular weight M-6.94 g/mol) metal among all metals. Because of its lightweight and small volume, lithium metal has an exceptionally high energy density. These characteristics suggest that metallic lithium is a good candidate for the anode-active material in rechargeable lithium batteries. Lithium metal, however, is inherently unstable. Furthermore, at high cycle numbers, the lithium metal utilized in the anode branches out towards the cathode, creating a short circuit that raises the battery's temperature to the point where it explodes.[42] Improvements in metal-free, low-cost, and environmentally friendly energy storage devices have resulted from using organic quinones as high-performance electroactive materials. On the cathode side of existing Li-ion battery systems, commercial electrode materials consist of lithium-containing transition metals, such as $LiCoO_2$, $LiFePO_4$, or $LiMn_2O_4$. In order to store Li ions, positive and negative

electrodes use host electrode materials that undergo intercalation reactions during the charging and discharging processes, respectively.[43,44] Li-ion conductive organic solvent is the electrolyte. Li ions are released during charging because of the layered nature of the metal oxide electrode. Together, the electrons flow from the positive to the negative electrode.[43,44](Figure 1.8)

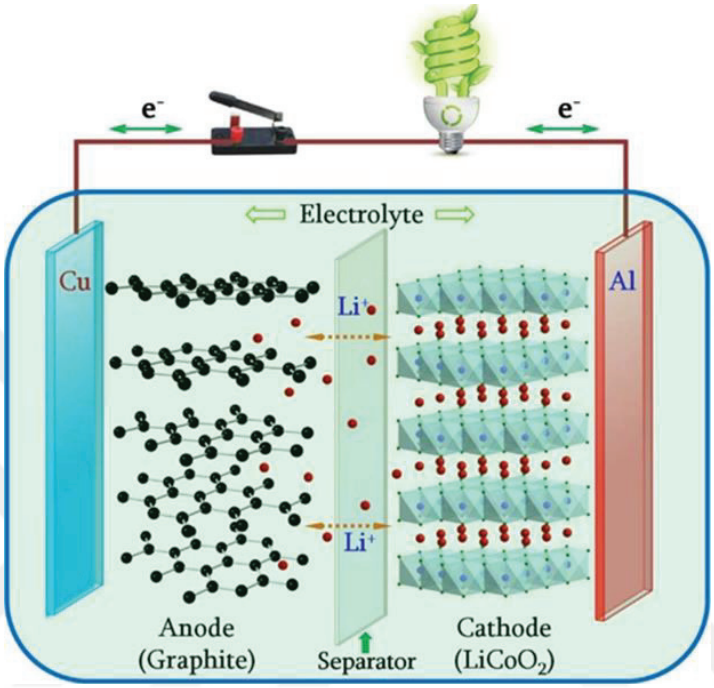

Figure 1.8 Schematic representation of a Li-ion Battery[43]

The cathode in a lithium battery is the site where lithium ions are accepted, whereas the anode provides the lithium. The cell voltage increases when the positive electrode voltage reaches its maximum and the negative electrode potential falls. The cell can now generate its own electrical energy. Last but not least, they repeatedly migrate between the electrodes.[43]

Ion mobility at an electrode and at the electrode interface, however, is too sluggish at high current densities for the charge distribution to attain equilibrium. As a result, the battery's reversible capacity decreases as the current density rises. Additionally, it explains why lowering the charge and/or discharge rate reduces capacity loss.[45]

However, some rational design strategies have been presented, offering high capacity and rate performance. In this regard, graphene-containing composites show high performance. Studies in the literature have shown that a particular capacity of 390 mAh/g is measured at a high current density of 1600 mA/g. (Fig.1.9). It was found to have a

capacity of 730 mAh/g when tested again at 400 mA/g after being tested at various current densities. These values are relatively high when compared to those of Mn_3O_4 by itself. In the same current range, the material has a specific capacity of 900 mAh/g, significantly higher than the capacity of less than 300 mAh/g for Mn_3O_4 alone. This highlights how the use of a highly conductive substance like graphene can significantly improve the efficiency of lithium batteries.[46]

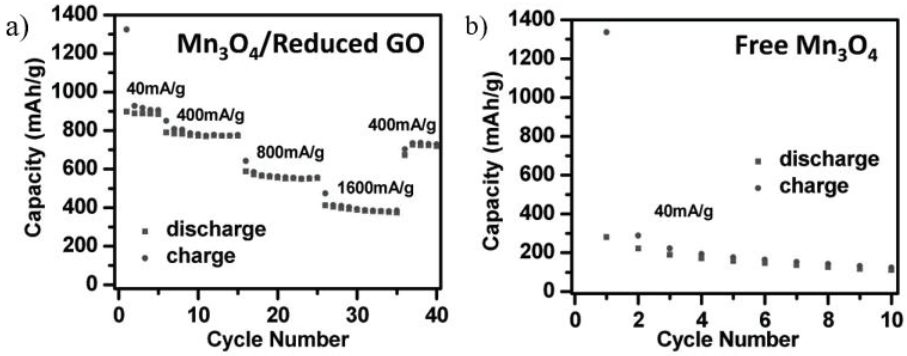

Figure 1.9 a) Capacity retention of Mn_3O_4/RGO at various current densities. b) The capacity retention of free Mn_3O_4 nanoparticles without graphene at a current density of 40 mA/g.[46]

In another study, the performances of graphene, Co_3O_4, and Co_3O_4/graphene composites were investigated by electrochemical tests. Initial discharge and charge capacities of 2179 and 955 mAh/g for graphene, 1105 and 817 mAh/g for Co_3O_4, and 1097 and 753 mAh/g for Co_3O_4/graphene composite were obtained.[47]

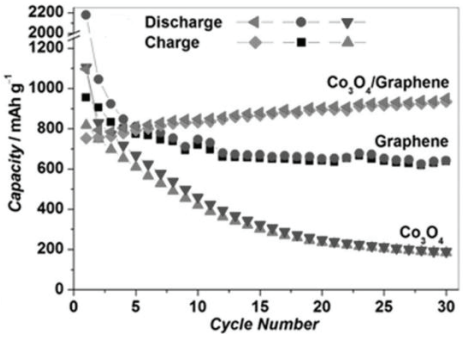

Figure 1.10. Capacity/cycle number of graphene, Co_3O_4, and Co_3O_4/graphene Composites.[47]

In another study, two different COF based active materials were synthesized from tetramino-benzoquinone (TABQ) and pyromellitic dianhydride (PMDA) with and without graphene (PIBN and PIBN-G, respectively). Multiple carbonyl redox groups in

PIBN and a 2D framework including 1.5 nm micropores provide high ion accommadation capacity and promote ion diffusion, respectively. On the other hand, the graphene-enhanced PIBN-G shows high electron conduction and low Li^+ diffusion resistance.[48]

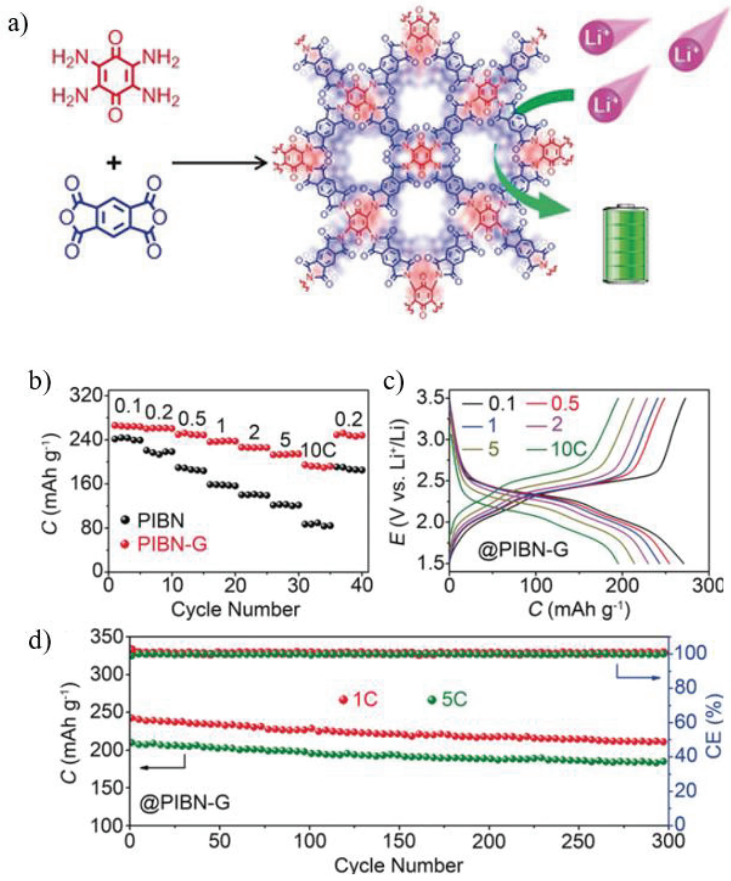

Figure 1.11. a) Schematic representation of the synthesis of polymer b) rate performance c) discharge/charge profiles d) cycle stability.[48]

It is clear that PIBN-G achieves better specific capacities at higher rates than PIBN. The strong interaction and charge transfer between PIBN and graphene support facilitate the rapid Li+ and electron transport in PIBN-G. PIBN-G provides initial capacities of 242.3 and 206.7 mAh g^{-1} at 1 and 5 C, respectively, and showed a slight decrease at 208.1 and 182.3 mAh g^{-1} after 300 cycles. The intense interaction between PIBN and graphene, as well as its carbonyl-rich and highly porous structure, are the reasons for its high specific capacity and rate capacity.[48]

1.8 Zinc-ion Batteries

The inherent disadvantages of lithium-ion batteries (LIBs), including high prices, toxic electrolytes, and safety issues, have led researchers to explore different types of batteries.[49-50] To avoid these growing concerns, rechargeable zinc batteries using aqueous electrolytes can be seen as an alternative to lithium-ion batteries.[51] Among the reported cathode materials for ZIBs, inorganic materials make up a large proportion, consisting of manganese-based oxides, vanadium-based oxides, and Prussian blue analogs, etc.[52-53] These materials have worked quite well in terms of Zn storage performance. However, the usage of inorganic cathode materials for ZIBs has been hampered by several issues. Inorganic materials, in which transition metal elements are commonly utilized, are harmful to humans and the environment due to their toxicity. Furthermore, the insertion of Zn^{2+} into layers of these inorganic materials, like manganese-based oxides, leads to volume change, and this expansion can cause collapsing of structure with increasing cycle number.[54] On the other hand, organic cathode materials are more eco-friendly, inexpensive, flexible (volume changes are minimal during discharge-charge), and lightweight than inorganic ones. It's also possible to shape their molecular composition.[55](Figure 1.12a)

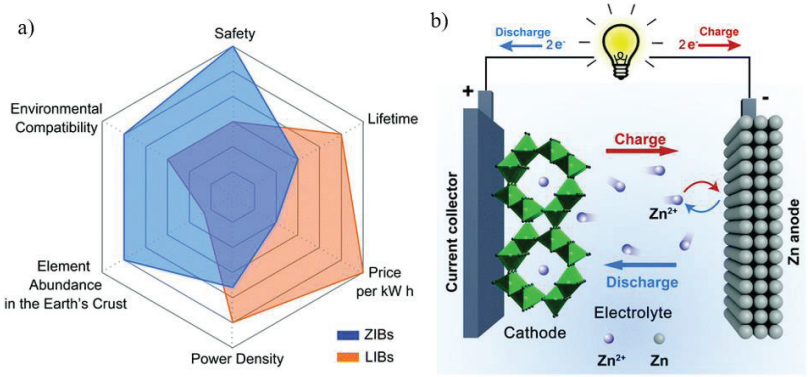

Figure 1.12 a) Comparison of zinc-ion and lithium-ion batteries. (b) Schematic representation of the working principle of zinc-ion batteries.[55]

ZIBs operate through reversible Zn^{2+} intercalation/deintercalation (cathode) and Zn coating/stripping (anode) upon discharge/charge.[56] In general, the aqueous solution of zinc-containing salts such as $ZnSO_4$, $Zn(CF_3SO_3)_2$, $Zn(CH_3COO)_2$ are used as electrolytes. Understanding the working mechanism of electrodes is crucial to develop

high-performance ZIBs.[57] In this respect, developing new organic cathodes and exploring their electrochemical properties is highly important.

1.8.1 Quinones

The energy storage mechanism of quinones as ZIB cathodes has received a great deal of attention. Quinones are highly redox activity and enolates are formed when the quinones (C=O) accept electrons, which can interact with Zn^{2+} ions. Some quinone-rich organic molecules have recently been reported as promising cathodes for ZIBs. One of the initial studies presented a series of small molecular quinone-based cathodes for ZIBs demonstrated good Zn storage performance. (Figure 1.13) While para-quinones show higher capacity, lower capacitance is seen for ortho-quinones. Figure (1.13a) Although the C4Q-based cathode exhibited good cycle stability, the usage of the complicated and expensive separator to eliminate the solubility of discharged product C4Q inhibits the practical application.[58]

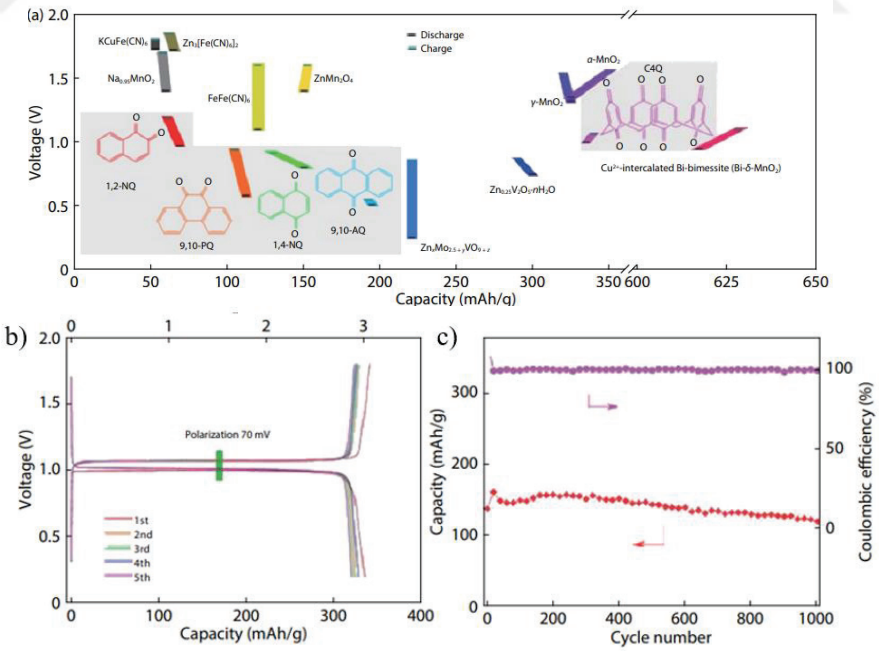

Figure 1.13 a) The voltages and capacities in zinc-ion batteries b) The charge discharge curves of Zn-C4Q c) cycling performance of Zn-C4Q at 0.5 A/g in ZIB[58]

POPs are notoriously insoluble in most common electrolytes. Consequently, it is anticipated that it will have high cyclability. In addition, the porous structure of porous polymers aids in the leaching and conversion of electrolytes, making them superior to linear polymers as electrode materials. For example, a HqTp covalent organic framework (COF) with a pore size of 1.5 nm was created, synthesized by the polycondensation of 2,5-diaminohydroquinone dihydrochloride (Hq) with 1,3,5-triformylphloroglucinol (Tp). It exhibited a remarkable specific capacity of 276 mAh/g high-capacity at a current density of 0.125 A/g. The cycle performance showed a capacity of 95% after 1000 cycles at 0.15 A/g.[59]

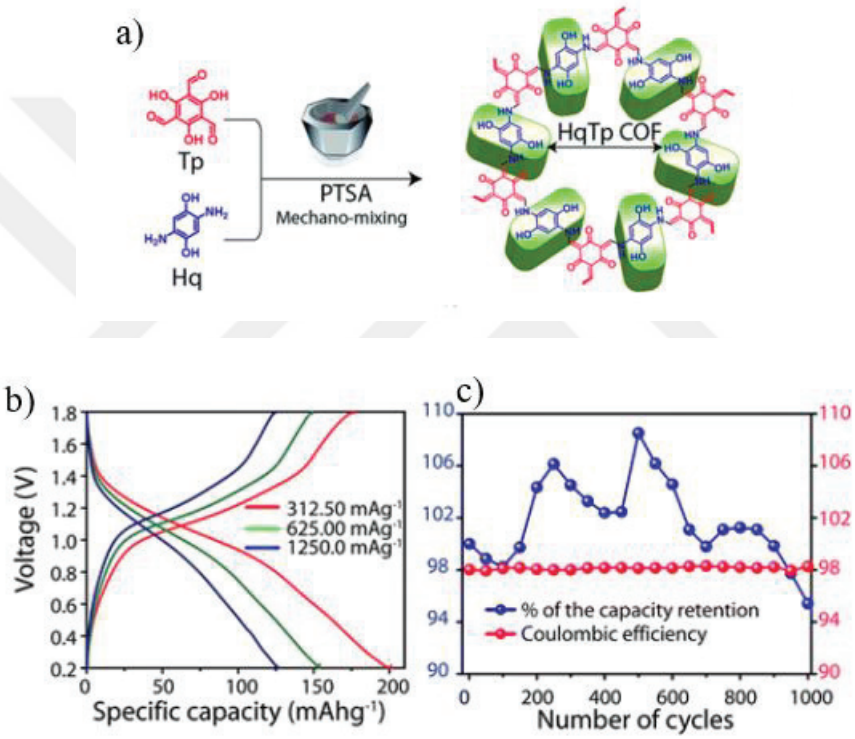

Figure 1.14 a) Schematic representation of the synthesis of HqTp b) Charge–discharge c) cyclic stability and coulombic efficiency plot [59]

CHAPTER 2

EXPERIMENTAL STUDY

2.1 General Methods

General: All chemicals and solvents were commercial grade and purchased from ABCR, Carlo Erba, Aldrich, and FluoroChem. Analytical thin-layer chromatography, often known as TLC, was performed on aluminum sheets that had been coated with silica gel 60-F254 (Merck 5554). Purifying the generated chemicals was accomplished by using flash column chromatography with Merck Kieselgel 60 H silica gel serving as the stationary phase. ^{1}H NMR and ^{13}C NMR spectra were recorded with a Varian 400 Nuclear Magnetic Resonance Spectrometer (400 MHz for ^{1}H NMR and 100 MHz for ^{13}C NMR) spectrometer. Coupling constants (J values) were reported in Hz. Chemical shifts were given in parts per million (ppm). $CHCl_3$ peaks were used as a reference in ^{1}H-NMR (7.26 ppm).

2.1.1 Powder X-ray Diffraction (XRD)

X-ray diffraction (XRD) patterns, a Philips X'Pert Pro model, were used to check the structural order of the synthesized compounds. Diffraction data were reported with 2Θ range 2°– 60°, which was collected with a step size of 0. 02, Cu-Kα (k = 0.154 nm) radiation at 45 kV and 40 mA value range. XRD graphics were plotted with the OriginPro-9.0 program.

2.1.2 Scanning Electron Microscope (SEM)

The particle morphology of the synthesized polymers were characterized using

scanning electron microscopy (SEM; ZEISS EVO10, MA1 operated at between 5 and 15 kV acceleration voltage). The elemental composition of the materials was explored by using the energy-dispersive X-ray (EDX).

2.1.3 Thermogravimetric Analysis (TGA)

The thermal stability of polymers was investigated using thermogravimetric analysis (TGA) by a Perkin Elmer Diomand TG/DTA. TGA thermograms have been collected with a heating rate of 10°C/min to 800 °C under a nitrogen atmosphere. The thermograms were collected using approximately 10 mg of powder of samples.

2.1.4 Brunauer-Emmett-Teller (BET)

The samples were made ready for analysis by being degassed for 12 h at 120 °C under vacuum. N_2 adsorption-desorption analysis was performed by Micromeritics Gemini V at 77 K. Using a Rouquerol plot, we were able to identify the relative pressure range corresponding to the exact BET surface area. To determine the total pore volume, the N_2 sorption isotherm was studied at relative pressures (P/P_0) ranging from 0.10 to 0.99.

2.1.5 Fourier Transform Infrared Spectrometer (FT-IR)

At room temperature and relative humidity, prepared KBr disks of synthesized polymers, model compounds and monomers were subjected to Fourier transform infrared spectroscopy (FT-IR), which was performed with a Perkin Elmer Spectrum 100 FT-IR spectrometer set to transmission mode.

2.2 Electrochemical Studies

2.2.1 Preparation of Cathode and Anode

In order to create a slurry or paste, the r-POPs were mixed with activated carbon particles (20%), which served as the conductive component; 10% tetrafluoroethylene (PTFE), which served as the binder; and ethanol, which served as the volatile solvent. After the remaining solvent had been removed, the pressed dough was rolled out and cut into little discs (each measuring 8 millimeters in diameter) using a press roller. The electrodes were then heated to 60 °C for 12 hours to remove the solvent. The anode material was punched zinc foil with a thickness of 0.025 millimeters to produce disks with a diameter of 8 millimeters. As the electrolyte for freshly prepared full cells of aqueous rechargeable ZIBs, a 3 M aqueous solution of $ZnSO_4$ was prepared and pre-degassed by argon purging prior to assembling the electrochemical cells. Swagelok cells were used to create the electrochemical cells. The Swagelok cells were filled, assembled, and caped in ambient conditions. The active substance loading was in the 2-4 mg cm^{-2} range. A Biologic SP 300 potentiostat and a LAND-CT3001A battery-testing apparatus were used to collect CV-curves and galvanostatic charge-discharge cycles for the fabricated ZIB cells cycled between 0.1 and 1.6/ 2.0 V.

2.3 Synthesis Section

2.3.1 Synthesis of diethyl 1,3,5,7-tetraoxo-1,2,3,5,6,7-hexahydro-s-indacene-2,6-dicarboxylate (Compound)

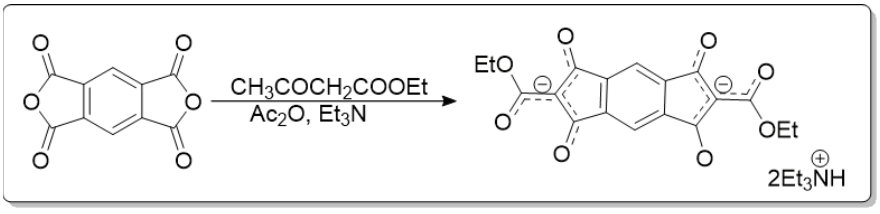

Compound was synthesized according to the literature.[60] Pyromellitic anhydride (2 g, 0.009 mol) was dissolved in a mixture of ethyl acetoacetate (3.5 ml 0.027 mol), triethylamine (7.7 ml, 0.054 mol) and acetic anhydride (16 mL). The mixture was heated at 70 °C for about 2 hours. After the reaction had reached room temperature, the final mixture was kept at 0–5 °C overnight. Then, the filtered solids were washed extensively with acetic anhydride and diethyl ether to afford orange solids as the desired product, Compound. ^{1}H NMR (400 MHz, $CDCl_3$) δ 7.6 (s, 2H), 4.2 (q, 4H), 3.25 (m, 12H), 1.4 (t, 6H), 1.3 (t, 18H).

2.3.2 Synthesis of s-indacene-1,3,5,7(2H,6H)-tetraone (Monomer)

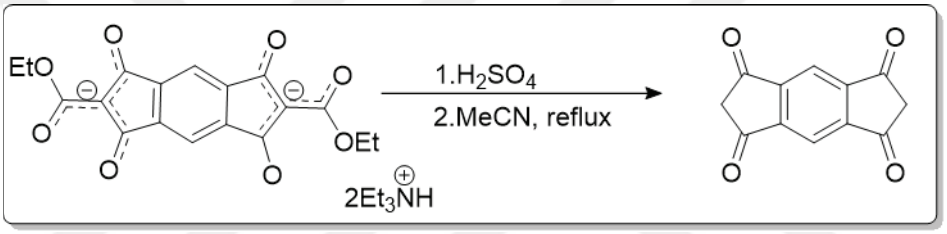

Monomer was also synthesized according to the literature.[60] Compound was added to a solution of H_2SO_4 (1 mL) and water (100 mL), which was cooled to 0°C using the cooling bath (water-ice mixture). Then the cooling bath was removed, the formed precipitates were filtered, washed extensively with EtOH, and dried at room temperature under a vacuum. Then, the dried solids were added to acetonitrile (20 ml) and heated under reflux for 2 hours. The precipitate was filtered, washed with acetonitrile and dried to give monomer (1.8 g, 90%) as a colorless solid. ^{1}H NMR (400 MHz, $CDCl_3$) δ 8.5 (s, 2H), 3.4 (s, 4H).

2.3.3 Synthesis of 2-benzylidene-1H-indene-1,3(2H)-dione (Model Compound)

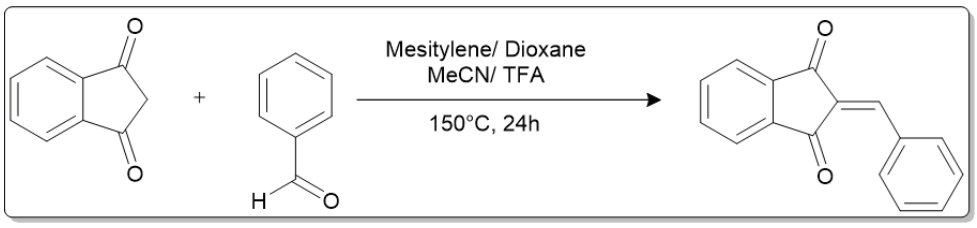

1,3-Indandione (200 mg, 1.36mmol), benzaldehyde (140µl, 1.36mmol), 3 mL mesitylene, 3 mL 1,4-dioxane, 1.3 mL trifluoroacetic acid, and 0.5 mL acetonitrile were added to a Schlenk tube. The reaction was heated at reflux at 150 °C for 24 hours to give a red solution. The product was purified using column chromatography to afford the model compound as a light-yellow solid (97%). (Hexane/Ethyl acetate =2:1). ^{1}H NMR (400 MHz, $CDCl_3$) δ 8.5 – 8.4 (m, 2H), 8.1 – 7.9 (m, 2H), 7.9 (s, 1H), 7.8 – 7.7 (m, 2H), 7.6 – 7.4 (m, 3H). ^{13}C NMR (100 MHz, $CHCl_3$) δ 190.2, 188.9, 146.9, 142.4, 140.0, 135.3, 135.1, 134.1, 133.1, 133.0, 129.1, 128.7, 123.3, 123.3.

2.3.4 Synthesis of redox-active porous organic polymer (r-POP) [Method-1]

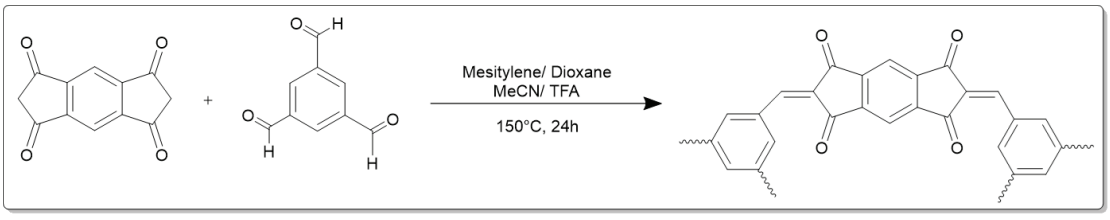

A solution of s-indacene-1,3,5,7(2H,6H)-tetraone (monomer) (33 mg, 0.15 mmol), benzene-1,3,5-tricarbaldehyde (16 mg, 0.09 mmol) and 0.45 mL mesitylene, 0.45 mL 1.4-dioxane, 0.025 ml acetonitrile, 0.2 mL trifluoroacetic acid prepared and added into a Pyrex ampule. After repeating the freezing-vacuum and thawing cycle at 78 K (liquid N_2 solution) three times, it was degassed and closed with flame under vacuum. It

was kept in an oven at 120 °C for 3 days. The precipitate formed was washed with methanol, water, and acetone. The resulting dark orange solid was dried under vacuum at 100 °C for 12 h to give r-POP (93.5mg, 73 % yield).

Synthesis of redox-active organic polymer (r-POP′) [Method-2]

A solution of s-indacene-1,3,5,7(2H,6H)-tetraone (monomer) (33 mg, 0.15 mmol), benzene-1,3,5-tricarbaldehyde (16 mg, 0.09 mmol) and p-toluene sulfonic acid (50 mg) prepared and added into a Pyrex ampule. Under nitrogen flow 1,2-dichlorobenzene (2.3 mL) and n-butanol (1 ml) were added. After repeating the freezing-vacuum and thawing cycle at 78 K (liquid N_2 solution) three times, it was degassed and closed with flame under vacuum. It was kept in an oven at 120 °C for 3 days. The precipitate formed was washed with methanol, water, and acetone. The resulting dark orange color solid was dried under vacuum at 100 °C for 12 h to give r-POP′ (98 mg, 76 % yield).

CHAPTER 3

RESULTS AND DISCUSSION

This study synthesized indandione-based redox-active porous organic polymers (r-POPs) via a condensation reaction between indandione-based monomers and 1,3,5-tricarboxybenzaldehyde. The most crucial feature of condensation reactions is that no metal-containing catalyst is needed. This makes these reactions not only environmentally friendly but also cost-effective. Also, quinone compounds are known for their low solubility, and to obtain a good polymerization, the high solubility of the oligomers formed is essential, as well as the efficiency of the reaction. Later, various optimization studies were carried out to obtain model compounds using redox-active molecules with monofunctional groups. Model compounds were characterized in detail using routine characterization techniques (NMR, MS, FTIR) as they are small organic compounds soluble in common organic solvents. Although model compounds can be used directly as potential electrode materials, they were used as reference materials to characterize r-POPs.

Regarding the reaction efficiency, reaction parameters (temperature, time, solvent etc.) were optimized using model compounds. Next, r-POPs were synthesized using the produced redox-active monomers and the necessary organic linkers. It was synthesized using different reaction strategies to increase the surface area and obtain a crystalline structure. Characterizations of r-POPs were investigated using various characterization techniques. At first, Fourier transforms infrared spectroscopy (FT-IR), scanning electron microscopy (SEM), gas adsorption analyzer (BET), and thermogravimetric analysis (TGA) analyzes were performed. The model compound and r-POPs obtained were electrochemically examined in detail. The performances of these synthesized polymeric materials were evaluated as cathodes for reversible aqueous ZIBs, and necessary optimizations were made within the information obtained. In addition to performance evaluations such as specific capacity and energy density, many electrochemical techniques were used to establish the structure-property relationship and to elucidate the working mechanisms.

3.1 Characterization and Electrochemical Studies

3.1.1 Characterization and electrochemical studies of redox active porous organic polymer (r-POP)

As mentioned above, we first synthesized the model compound to optimize the polymerization conditions. Then, r-POPs were synthesized with affordable yields by following similar reaction conditions in synthesizing the model compound. However, we have also investigated the effect of acid on polymerization and its effect on the textural properties of polymers. Therefore, we synthesized two r-POPs using different acids and solvent mixtures. A BET surface area of 169 $m^2 g^{-1}$ was observed for the polymer (r-POP) synthesized with mesitylene/dioxane/TFA/acetonitrile solvents. According to IUPAC classification, it shows a mixture of type-I and type-II isotherms. We can see a sharp increase in the low-pressure range which can be attributed to the presence of micropores. The sharp increase in the high-pressure region also indicates the existence of macropores. (Figure 3.1) The Rouquerol method was calculated to estimate the valid pressure range for the calculation of BET surface area. According to the Rouquerol plot, the pressure range used was calculated according to the adsorption data up to the maximum P/P_0 pressure of V $(1 - P/P_0)$. Adsorption beyond this value refers to the region where the amount adsorbed increases more slowly with pressure than the first adsorbed layer. (Figure 3.2)

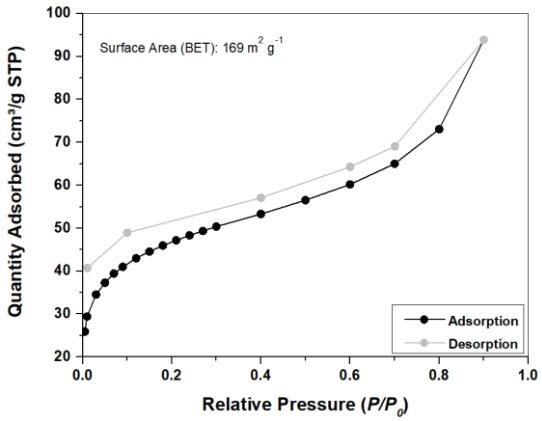

Figure 3.1. N_2 adsorption–desorption isotherm of r-POP measured at 77 K.

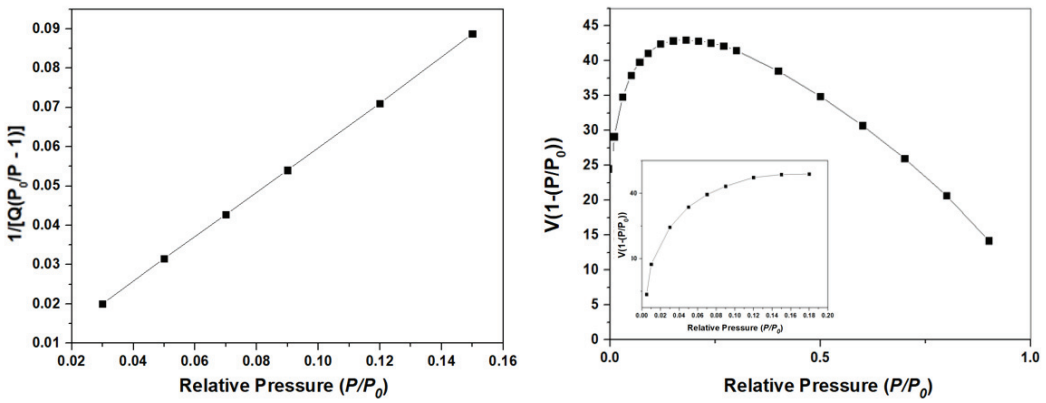

Figure 3.2. BET surface area and Rouquerol plot of r-POP.

The surface area of 194 m^2 g^{-1} was observed for the polymer synthesized using different acid catalysts (p-TsOH) and solvent systems (n-BuOH / o-DCB). The adsorption-desorption isotherm of r-POP shows a mixture of type I and type II isotherms. The steep increase in the low-pressure range indicates the presence of the type I isotherm (micropores smaller than 2 nm). Therefore, the micropores are filled, a monolayer is formed, and then a multi-layer coating is followed by liquefaction. (Figure 3.3 and Figure 3.4)

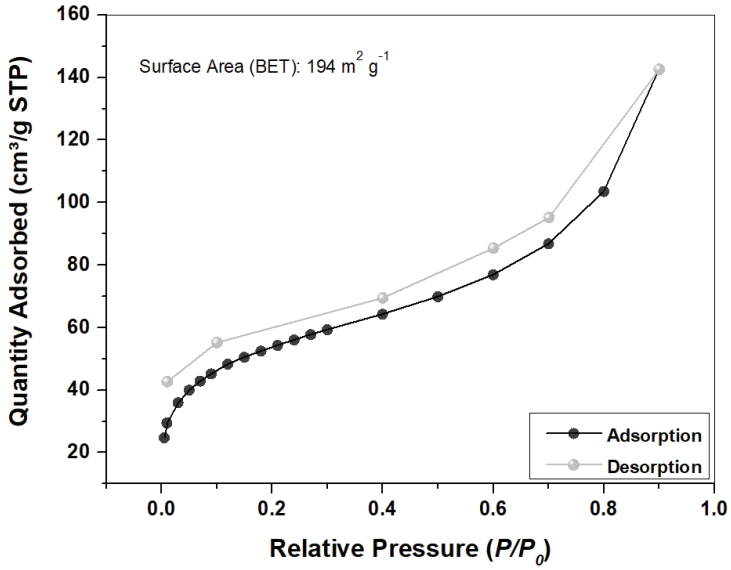

Figure 3.3. N_2 adsorption–desorption isotherm of r-POP′ measured at 77 K.

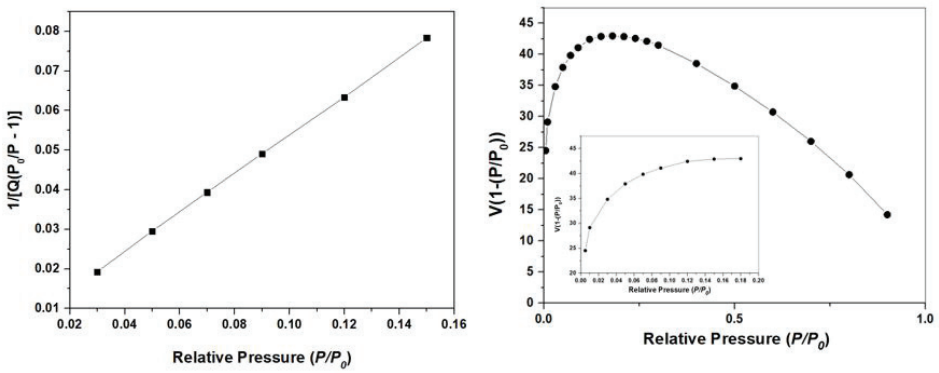

Figure 3.4. BET surface area and Rouquerol plot of r-POP′.

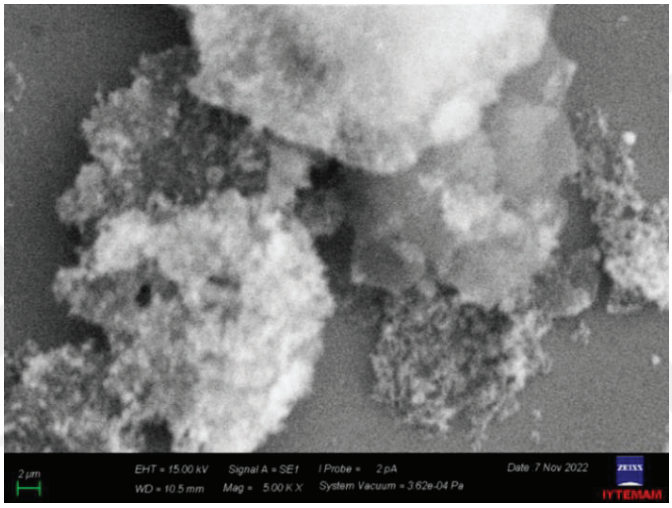

Figure 3.5. SEM images of r-POP.

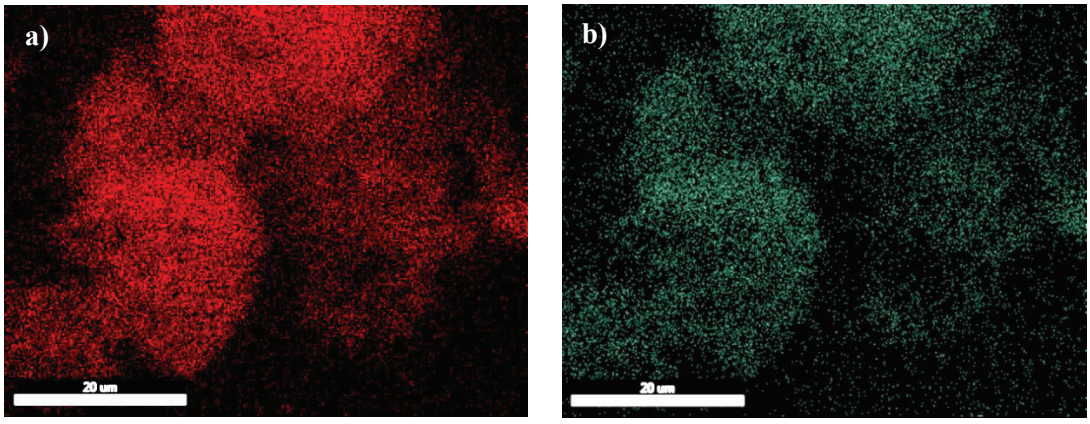

Figure 3.6. The corresponding EDX map of r-POP a) carbon b) oxygen

Particle morphology and surface images were examined using scanning electron microscopy (SEM). The 2 µm image of the synthesized material is shown in Figure 3.5. The surface image of the polymer has been reduced 500 times. EDX image was taken to

understand whether it has a homogeneous structure. It is observed that the polymer has a porous, homogeneous, and spherical-like structure. These structural features are in good agreement with the porosity measurements. Elemental mapping by EDX shows the homogeneous distribution of carbon and oxygen atoms in the structure of the polymer. (Figure 3.6.)

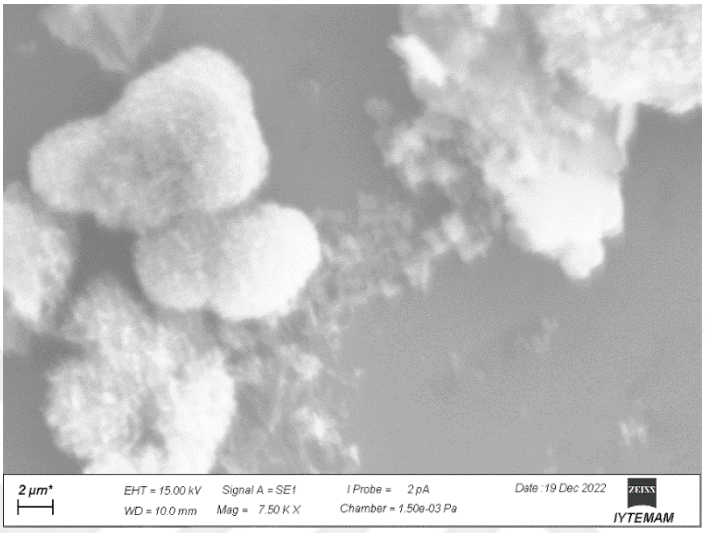

Figure 3.7. SEM images of r-POP′.

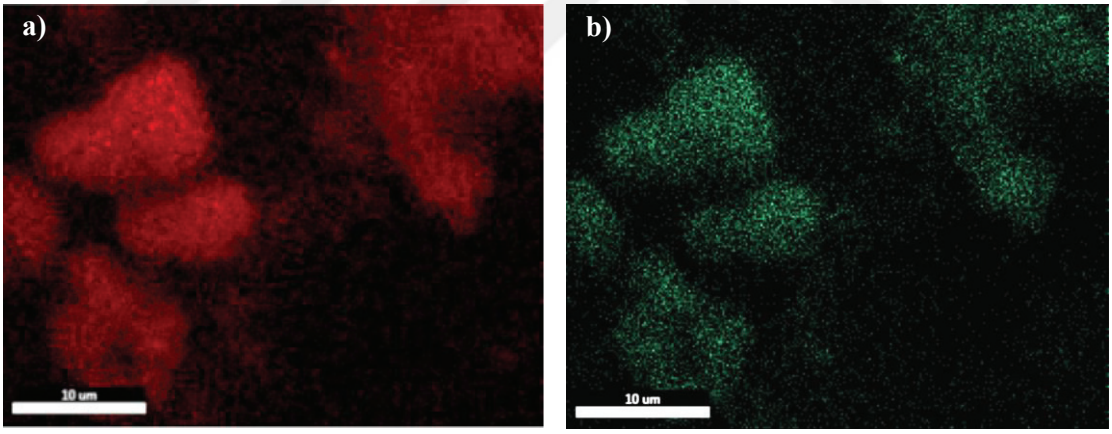

Figure 3.8. The corresponding EDX map of r-POP′ a) carbon b) oxygen

Particle morphology and surface images were examined using SEM. The SEM image of the synthesized material is shown in Figure 3.7. The SEM image shows that the r-POP' has spherical-like particles. As a result of BET analysis, it has been proven to have a porous structure that is consistent with SEM images. Elemental mapping with EDX shows the homogeneous distribution of carbon and oxygen atoms in the structure of the polymer. (Figure 3.8.)

The thermogravimetric analysis was performed at a speed of 10 °C/min up to

800°C in a nitrogen atmosphere. According to TGA measurements, the r-POP shows thermal stability up to 250°C. However, it lost about 15% of its weight at 350°C. Then there was a loss of about 60 % of its weight at 675 °C. (Figure 3.9)

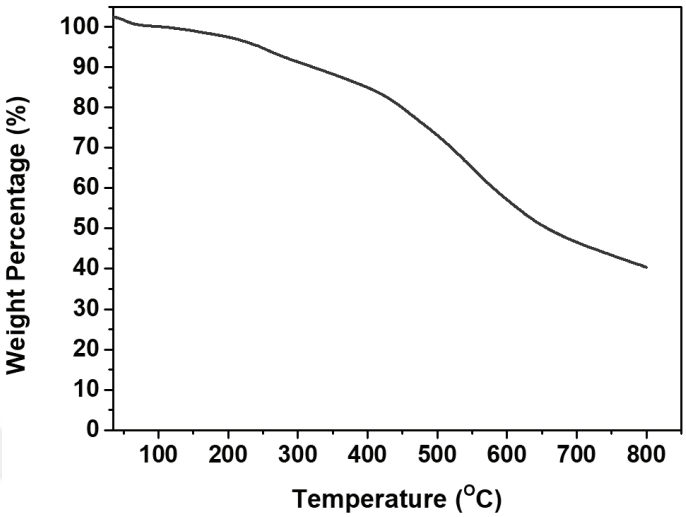

Figure 3.9 Thermogravimetric analysis (TGA) curves of r-POP.

The thermogravimetric analysis was performed at a speed of 10 °C/min up to 800°C in a nitrogen atmosphere. According to TGA measurements, the r-POP′ shows thermal stability up to 250°C. However, it lost about 15% of its weight at 350°C. Then there was a loss of about 70 % of its weight at 750 °C. (Figure 3.10)

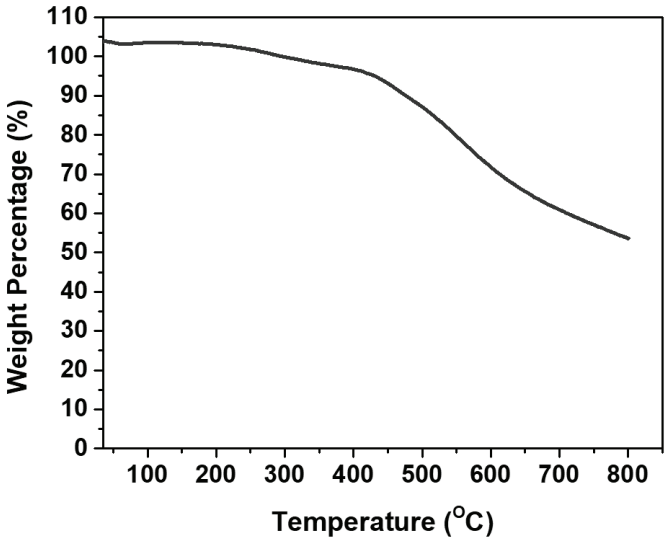

Figure 3.10 Thermogravimetric analysis (TGA) curves of r-POP′.

The molecular structure of the synthesized polymers was characterized by FT-IR spectroscopy. The model compound was used as a reference in the characterization of the polymers. As shown in Figure 3.11, the comparative FT-IR spectrum with the model compound clearly shows vibrational bands of C=O (approximately 1700 cm^{-1}) and C=C (1550 cm^{-1}) bonds at similar wavelengths. The band gap at 1692 cm^{-1} corresponds to both structures -C=O bond. 1650 cm^{-1} stretching vibration corresponds to C=C bonds. The FT-IR results show that the polymer has been successfully synthesized.

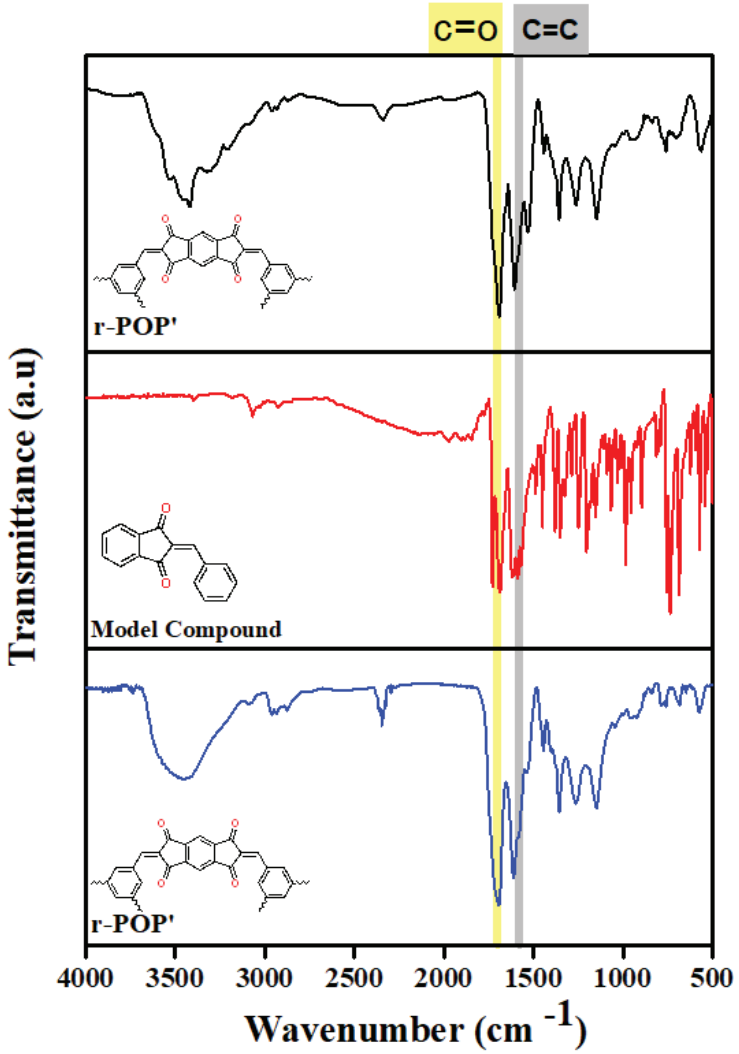

Figure 3.11. FTIR spectra of the model compound, r-POP and r-POP′.

Polymers were synthesized under various solvent mixtures and reaction conditions. To obtain the most thermodynamically stable and ordered structure. However, despite many attempts, the absence of a significant peak in the XRD analysis as shown in Figure 3.12 indicates that the structure does not show crystallinity and has an amorphous structure.

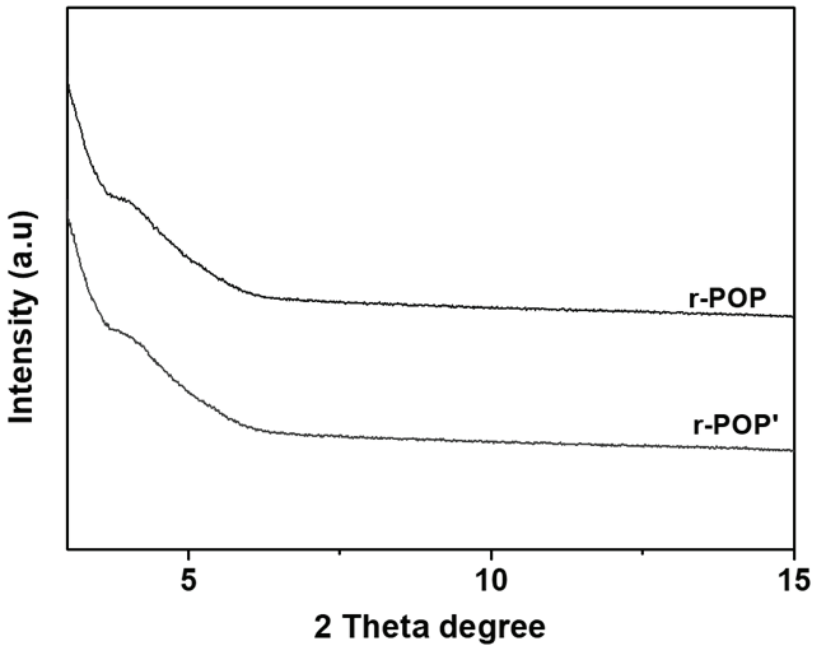

Figure 3.12. X-ray diffraction (XRD) pattern of r -POP, r -POP′.

The electrochemical properties of the polymers were evaluated using several techniques. To explore the oxidation and reduction potentials of the polymers, the cyclic voltammograms was collected at different scan rates in 3M $ZnSO_4$ solution between the voltage range of 0.1 and 2.0 V. We firstly collected r-POP's CV curves. Two oxidation peaks were observed at about 0.6 and 1.1 V and one reduction peak was observed at 0.8 V. (Figure3.13). As shown in Figure 3.14, CV curves of r-POP′ was collected at different scan rates in 3M $ZnSO_4$ solution between the voltage range of 0.1 and 2.0 V. In consistent with r-POP, r-POP′ also shows two oxidation and one reduction peaks, which two oxidation peaks were observed at about 0.6 and 1.1 V and one reduction peak was observed at 0.8 V. (Figure3.14)

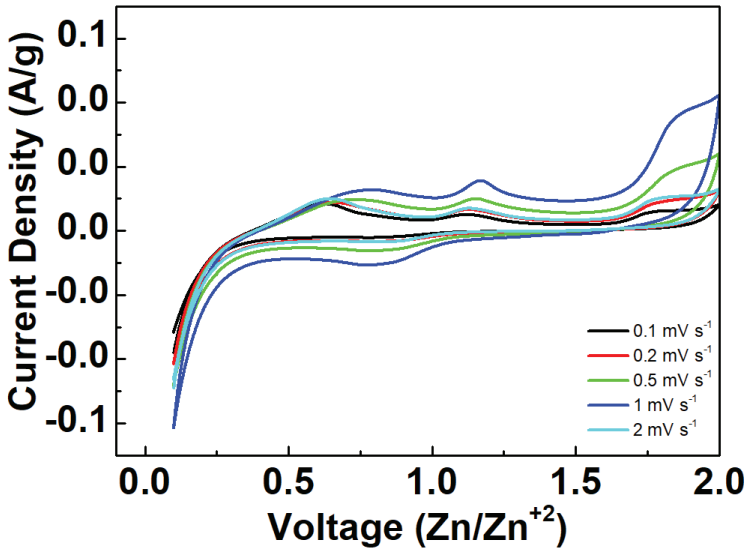

Figure 3.13. CV curves of r-POP.

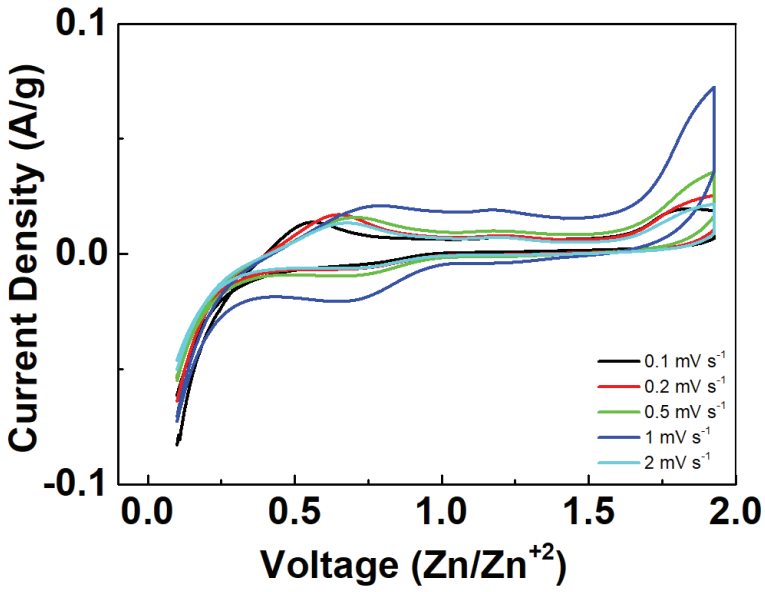

Figure 3.14. CV curves of r-POP′.

The Figure 3.14 shows cyclic voltammograms of the Zn electrode in the aqueous electrolyte with varying $ZnSO_4$ concentrations. Evaluated at various scan rates (0.1 - 2 mV s^{-1}) to estimate capacitance values. A higher capacitance value is observed for a low scan rate than for a high scan rate. No active redox points were observed. CV curves at different scanning rates at different voltage ranges, and redox peaks in both electrode systems indicate very low redox kinetics in the electrochemical system.

The galvanostatic charge/discharge profiles of r-POP was collected at different current densities. It is shown that the charge/discharge capacities depend on the applied

current densities. At a low current density of 0.1 A g^{-1}, the specific discharge capacity increased to 1.4 mAh g^{-1}. However, when a high current density such as 1 A g^{-1} was applied, it decreased to 0.6 mAh g^{-1}. No flat and distinct voltage plateau was observed in any of the charge/discharge curves, and it shows sloping charge-discharge curves. The GCD results are consistent with the CV curves shown in the Figure 3.15.

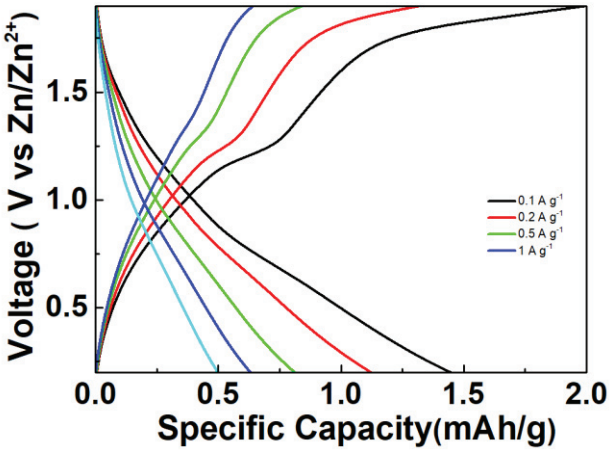

Figure 3.15. Galvanostatic charge/discharge profiles at different current densities of r-POP.

Furthermore, the galvanostatic charge/discharge profiles of r-POP′ was collected at different current densities. At a low current density of 0.1 A g^{-1}, the specific discharge capacity is 2.6 mAh g-^{1}. However, when a high current density such as 1 A g^{-1} was applied, it decreased to 0.4 mAh g^{-1}. No distinct voltage plateau was either observed in any of the charge/discharge curves of r-POP′. The galvanostatic charge/discharge profiles are consistent with the CV curves shown in Figure 3.16.

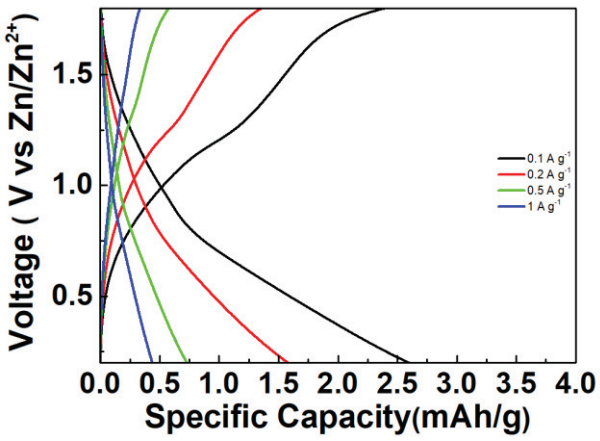

Figure 3.16. Galvanostatic charge/discharge profiles at different current densities of r-POP′.

The rate performance of r-POP and r-POP' measured at various current densities ranging from 0.1 to 20 A g^{-1} is shown in Figure 3.17. The specific capacity of the r-POP' electrode is better than that of the r-POP electrode at any current density. The capacitance for r-POP' shows a value of about 3.5 mA g^{-1} on the first cycle, but for r-POP this value is about 1.6 mA g^{-1}. As the current density increases, the capacity of polymers decreases. (Figure 3.17- Figure 3.18)

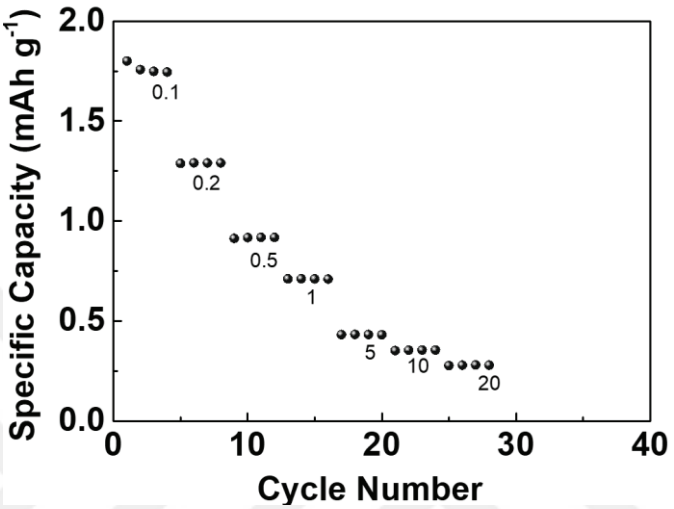

Figure 3.17. Rate (charge-discharge) performance of r-POP under various current densities.

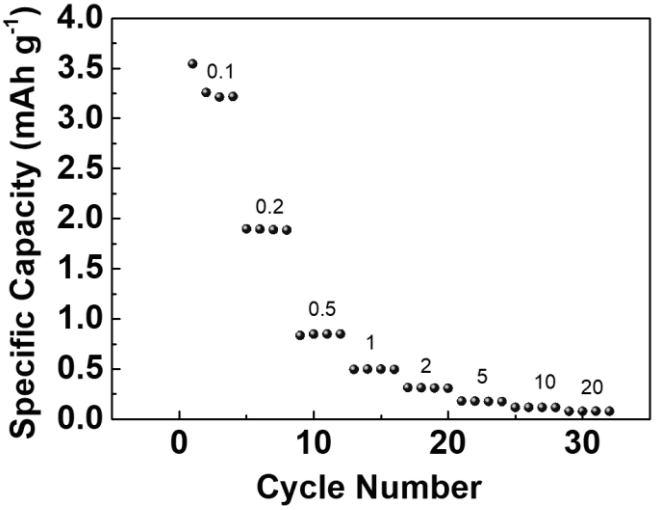

Figure 3.18. Rate (charge-discharge) performance of r-POP′ under various current densities.

To understand the electrochemical kinetics of the electrodes, the change in peak current with the applied scan rate is examined and is shown in Figure 3.19 and Figure

3.20. The slope of the linear plot of log *v* versus log *i* provides the value of coefficient b, which governs the charge storage mechanism. A value of b = 1 indicates a pseudo-capacitive material involving surface redox-mediated reactions, and a value of b = 0.5 describes it as a battery-type material with diffusion-controlled processes. While the slope close to 0.5 is explained for the diffusion-controlled process, the slope close to 1.0 is explained for the capacitive-controlled process. The slope of the four dependencies is between 0.5 and 1.0, which explains the joint control of diffusion and adsorption. The b-values for the corresponding peaks for r-POP are 0.67 and 0.69, which indicates that the diffusive controlled charge storage mechanism is dominant over capacitive contribution. On the other hand, b-values for r-POP′ are 0.76 and 0.78, which are higher than r-POP, suggesting the capacitive contribution is much greater than r-POP. This difference in capacitive contribution can be originated from the difference in surface area and porosity. The higher porosity and large surface area of r-POP′ provide more sites for pseudo capacitance and result in higher contribution from capacitive charge storage process.

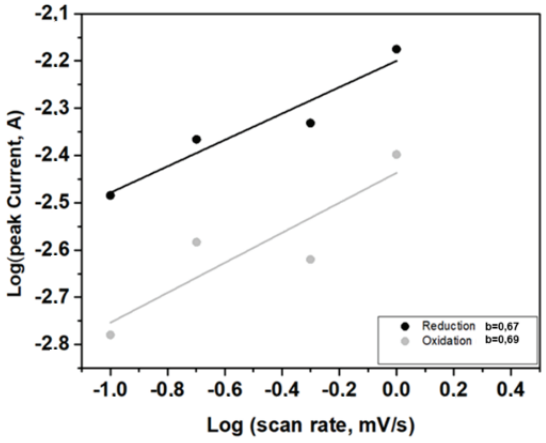

Figure 3.19. Logarithmic relationship of peak current and scan rate of r-POP.

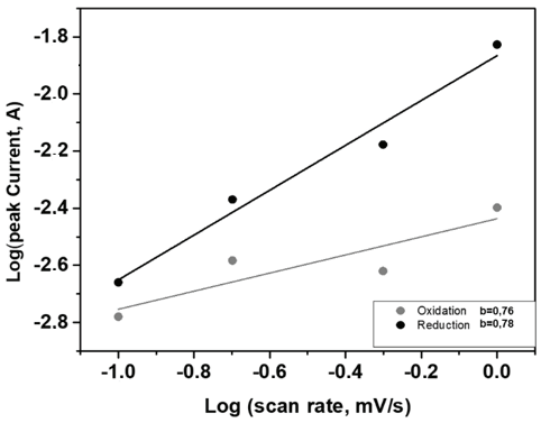

Figure 3.20. Logarithmic relationship of peak current and scan rate of r-POP′.

CHAPTER 4

CONCLUSION

This study used low-cost, environmentally friendly redox-active indandione based porous organic polymers (r-POP) as cathode-active material in zinc-ion batteries. Indandione-based POPs prepared by an acid-catalyzed condensation reaction between s-indacene-1,3,5,7(2H,6H)-tetraone and benzene-1,3,5-tricarboxaldehyde. These polymers were characterized using various characterization techniques, including FT-IR, XRD, SEM, EDX, TGA, and gas adsorption analysis.

FT-IR spectra of the model compound and polymers show consistency and support the polymers' successful synthesis. They have high surface areas up to 169 $m^2 g^{-1}$ and 194 $m^2 g^{-1}$ of r-POP and r-POP′, respectively. They show high thermal stability up to 300 ^oC. SEM-EDX analysis further supports the successful synthesis of polymers, which offer homogeneous carbon (C) and oxygen (O) distribution. Although there are broad peaks, the XRD pattern of polymers suggests the lack of long-range order. The polymers were tested as cathode material for aqueous rechargeable ZIBs. The galvanostatic charge-discharge curves in the voltage range of 0.1 to 2.0 V at a current density of 0.1 A g^{-1} show low specific capacities of 1.5 and 2.5 mAh g^{-1} for r-POP and r-POP′. These capacities decrease more with increasing current densities. One of the main reasons for the low electrochemical performance of the synthesized polymeric structures is that Zn^{2+} ions cannot access the polymers redox-activate carbonyl groups, and the voltage window is limited due to the aqueous electrolyte used. In addition, due to the structural properties of r-POPs, their hydrophobicity, relatively low porosity, and small pore size could prevent the interaction of Zn^{2+} with embedded redox-active groups. Although they show low electrochemical performance, synthesizing indandione-based POPs has been successfully completed for the first time, and we believe the findings will inspire further studies.

REFERENCES

1. Salkuti, Surender Reddy. “Comparative Analysis of Electrochemical Energy Storage Technologies for Smart Grid.” *TELKOMNIKA (Telecommunication Computing Electronics and Control)* 18, no. 4 (2020): 2118.
2. Yuan, Xinhai. “Latest Advances in High-Voltage and High-Energy-Density Aqueous Rechargeable Batteries.” *SpringerLink*, September 1, 2020.
3. Pigłowska, Marita, Beata Kurc, Maciej Galiński, Paweł Fuć, Michalina Kamińska, Natalia Szymlet, and Paweł Daszkiewicz. “Challenges for Safe Electrolytes Applied in Lithium-Ion Cells—A Review.” *Materials* 14, no. 22 (2021): 6783.
4. Wan, Fang, and Zhiqiang Niu. “Design Strategies for Vanadium-based Aqueous Zinc-Ion Batteries.” *Angewandte Chemie* 131, no. 46 (2019): 16508–17.2019.
5. Ni, Qiao, Heng Jiang, Sean Sandstrom, Ying Bai, Haixia Ren, Xianyong Wu, Qiubo Guo, Dongxu Yu, Chuan Wu, and Xiulei Ji. “A $Na_3V_2(PO_4)_2O_{1.6}F_{1.4}$ Cathode of Zn-Ion Battery Enabled by a Water-in-Bisalt Electrolyte.” *Advanced Functional Materials* 30, no. 36 (2020): 2003511..
6. Wu, Dingcai, Fei Xu, Bin Sun, Ruowen Fu, Hongkun He, and Krzysztof Matyjaszewski. “Design and Preparation of Porous Polymers.” *Chemical Reviews* 112 no. 7 (2012): 3959–4015.
7. Thommes, Matthias, Katsumi Kaneko, Alexander V. Neimark, James P. Olivier, Francisco Rodriguez-Reinoso, Jean Rouquerol, and Kenneth S.W. Sing. “Physisorption of Gases, with Special Reference to the Evaluation of Surface Area and Pore Size Distribution (IUPAC Technical Report).” *Pure and Applied Chemistry* 87 no. 9-10 (2015): 1051–69.
8. Cote, A. P. 2005“Porous, Crystalline, Covalent Organic Frameworks.” *Science* 310 (5751): 1166–70.
9. Xu, Shujun, Yali Luo, and Bien Tan. “Recent Development of Hypercrosslinked Microporous Organic Polymers.” *Macromolecular Rapid Communications* 34 no.6 (2013): 471–84.
10. Katekomol, Phisan, Jérôme Roeser, Michael Bojdys, Jens Weber, and Arne Thomas. “Covalent Triazine Frameworks Prepared from 1,3,5-Tricyanobenzene.” *Chemistry of Materials* 25 no.9 (2013): 1542–48.

11. Tian, Yuyang, and Guangshan Zhu. “Porous Aromatic Frameworks (PAFs).” *Chemical Reviews* 120 no. 16 (2020): 8934–86.
12. Jiang, Jia-Xing, Fabing Su, Abbie Trewin, Colin D. Wood, Neil L. Campbell, Hongjun Niu, Calum Dickinson, et al.“Conjugated Microporous Poly(Aryleneethynylene) Networks.” *Angewandte Chemie* 119 no.45 (2007): 8728–32.
13. Feng, Xiao, Xuesong Ding, and Donglin Jiang. “Covalent Organic Frameworks.” *Chemical Society Reviews* 41 no.18 (2012): 6010.
14. Wan, Shun, Felipe Gándara, Atsushi Asano, Hiroyasu Furukawa, Akinori Saeki, Sanjeev K. Dey, Lei Liao, et al. “Covalent Organic Frameworks with High Charge Carrier Mobility.” *Chemistry of Materials* 23 no.18 (2011): 4094–97.
15. Huang, Ning, Ping Wang, and Donglin Jiang. “Covalent Organic Frameworks: A Materials Platform for Structural and Functional Designs.” *Nature Reviews Materials* 1 no.10 (2016).
16. Wu, Xiaowei, Xing Han, Yuhao Liu, Yan Liu, and Yong Cui. “Control Interlayer Stacking and Chemical Stability of Two-Dimensional Covalent Organic Frameworks via Steric Tuning.” *Journal of the American Chemical Society* 140 no.47 (2018): 16124–33.
17. Spitler, Eric L., and William R. Dichtel. “Lewis Acid-Catalysed Formation of Two-Dimensional Phthalocyanine Covalent Organic Frameworks.” *Nature Chemistry* 2 no.8 (2010): 672–77.
18. Gascon, J., J. R. van Ommen, J. A. Moulijn, and F. Kapteijn. “Structuring Catalyst and Reactor – an Inviting Avenue to Process Intensification.” *Catalysis Science & Technology* 5 no.2 (2015): 807–17.
19. Abuzeid, Hesham R., Ahmed F.M. EL-Mahdy, and Shiao-Wei Kuo.“Covalent Organic Frameworks: Design Principles, Synthetic Strategies, and Diverse Applications.” *Giant* 6 (2021): 100054.
20. Kandambeth, Sharath, Vinayak S. Kale, Osama Shekhah, Husam N. Alshareef, and Mohamed Eddaoudi. “2D Covalent-Organic Framework Electrodes for (2021), 2100177.
21. Ritchie, Lyndsey K., Abbie Trewin, Aida Reguera-Galan, Tom Hasell, and Andrew I. Cooper. “Synthesis of COF-5 Using Microwave Irradiation and Conventional Solvothermal Routes.” *Microporous and Mesoporous Materials* 132 no.1-2 (2010): 132–36.

22. Colson, John W., Arthur R. Woll, Arnab Mukherjee, Mark P. Levendorf, Eric L. Spitler, Virgil B. Shields, Michael G. Spencer, Jiwoong Park, and William R. Dichtel. “Oriented 2D Covalent Organic Framework Thin Films on Single-Layer Graphene.” *Science* 332 no. 6026 (2011): 228–31.
23. Li, Yingwei, and Ralph T. Yang. “Hydrogen Storage in Metal-Organic and Covalent-Organic Frameworks by Spillover.” *AIChE Journal* 54 no.1 (2007): 269–79.
24. Ding, San-Yuan, Jia Gao, Qiong Wang, Yuan Zhang, Wei-Guo Song, Cheng-Yong Su, and Wei Wang. “Construction of Covalent Organic Framework for Catalysis: Pd/COF-LZU1 in Suzuki–Miyaura Coupling Reaction.” *Journal of the American Chemical Society* 133 no.49 (2011): 19816–22.
25. Wang, Wenjing, Mi Zhou, and Daqiang Yuan. “Carbon Dioxide Capture in Amorphous Porous Organic Polymers.” *Journal of Materials Chemistry A* 5 no.4 (2017) : 1334–47.
26. Furukawa, Hiroyasu, and Omar M. Yaghi. “Storage of Hydrogen, Methane, and Carbon Dioxide in Highly Porous Covalent Organic Frameworks for Clean Energy Applications.” *Journal of the American Chemical Society* 131 no.25 (2009): 8875–83.
27. Ozdemir, John, Imann Mosleh, Mojtaba Abolhassani, Lauren F. Greenlee, Robert R. Beitle, and M. Hassan Beyzavi. “Covalent Organic Frameworks for the Capture, Fixation, or Reduction of CO_2.” *Frontiers in Energy Research* 7 (2019).
28. Lee, Jiyoung, Onur Buyukcakir, Tae-woo Kwon, and Ali Coskun.“Energy Band-Gap Engineering of Conjugated Microporous Polymers via Acidity-Dependent in Situ Cyclization.” *Journal of the American Chemical Society* 140 no.35(2018): 10937–40.
29. Luo, Songhao, Zhuotong Zeng, Han Wang, Weiping Xiong, Biao Song, Chengyun Zhou, Abing Duan, et al.“Recent Progress in Conjugated Microporous Polymers for Clean Energy: Synthesis, Modification, Computer Simulations, and Applications.” *Progress in Polymer Science* 115 (2021): 101374.
30. Xu, Yanhong, Shangbin Jin, Hong Xu, Atsushi Nagai, and Donglin Jiang. “Conjugated Microporous Polymers: Design, Synthesis and Application.” *Chemical Society Reviews* 42 no.20 (2013): 8012.
31. Holst, James R., StöckelEv, Dave J. Adams, and Andrew I. Cooper.“High Surface Area Networks from Tetrahedral Monomers: Metal-Catalyzed Coupling, Thermal Polymerization, and ‘Click’ Chemistry.” *Macromolecules* 43 no.20 (2010): 8531–38.

32. Schwab, Matthias Georg, Birgit Fassbender, Hans Wolfgang Spiess, Arne Thomas, Xinliang Feng, and Klaus Müllen. “Catalyst-Free Preparation of Melamine-Based Microporous Polymer Networks through Schiff Base Chemistry.” *Journal of the American Chemical Society* 131 no.21 (2009): 7216–17.
33. Taskin, Omer Suat, Sajjad Dadashi-Silab, Baris Kiskan, Jens Weber, and Yusuf Yagci. “Highly Efficient and Reusable Microporous Schiff Base Network Polymer as a Heterogeneous Catalyst for CuAAC Click Reaction.” *Macromolecular Chemistry and Physics* 216 no.16 (2015): 1746–53.
34. Xu, Yanhong, Shangbin Jin, Hong Xu, Atsushi Nagai, and Donglin Jiang. “Conjugated Microporous Polymers: Design, Synthesis and Application.” *Chemical Society Reviews* 42 no. 20 (2013): 8012.
35. Chaoui, Nicolas, Matthias Trunk, Robert Dawson, Johannes Schmidt, and Arne Thomas. “Trends and Challenges for Microporous Polymers.” *Chemical Society Reviews* 46 no.11 (2017): 3302–21.
36. Benoy, Santhi Maria, Mayank Pandey, Dhrubajyoti Bhattacharjya, and Binoy K. Saikia. “Recent Trends in Supercapacitor-Battery Hybrid Energy Storage Devices Based on Carbon Materials.” *Journal of Energy Storage* 52 (2022): 104938.
37. Kang, Narae, Ji Hoon Park, Mingshi Jin, Nojin Park, Sang Moon Lee, Hae Jin Kim, Ji Man Kim, and Seung Uk Son.“Microporous Organic Network Hollow Spheres: Useful Templates for Nanoparticulate Co_3O_4 Hollow Oxidation Catalysts.” *Journal of the American Chemical Society* 135 no.51 (2013): 19115–18.
38. Khamsanga, Sonti, Rojana Pornprasertsuk, Tetsu Yonezawa, Ahmad Azmin Mohamad, and Soorathep Kheawhom.“δ-MnO_2 Nanoflower/Graphite Cathode for Rechargeable Aqueous Zinc Ion Batteries.” *Scientific Reports* 9 no.1 (2019).
39. Liu, Huanyan, Jian-Gan Wang, Zongyuan You, Chunguang Wei, Feiyu Kang, and Bingqing Wei. “Rechargeable Aqueous Zinc-Ion Batteries: Mechanism, Design Strategies and Future Perspectives.” *Materials Today* 42 (2021): 73–98.
40. Lu, Yi-Chun, David G. Kwabi, Koffi P. C. Yao, Jonathon R. Harding, Jigang Zhou, Lucia Zuin, and Yang Shao-Horn.“The Discharge Rate Capability of Rechargeable Li–O_2 Batteries.” *Energy & Environmental Science* 4 no. 8 (2011): 2999.
41. Buchmann, Isidor, and Cadex Electronics Inc. 1997. *Batteries in a Portable World*. Ec & M Books.
42. Tarascon, J.-M., and M. Armand. “Issues and Challenges Facing Rechargeable Lithium Batteries.” *Nature* 414 no.6861 (2001): 359–67.

43. Liu, Chaofeng, Zachary G. Neale, and Guozhong Cao. “Understanding Electrochemical Potentials of Cathode Materials in Rechargeable Batteries.” *Materials Today* 19 no.2 (2016): 109–23.
44. Han, Cuiping, Hongfei Li, Ruiying Shi, Tengfei Zhang, Jing Tong, Junqin Li, and Baohua Li. “Organic Quinones towards Advanced Electrochemical Energy Storage: Recent Advances and Challenges.” *Journal of Materials Chemistry A* 7 no.41 (2019): 23378–415.
45. Goodenough, John B., and Youngsik Kim. “Challenges for Rechargeable Li Batteries.” *Chemistry of Materials* 22 no.3 (2010): 587–603.
46. Wang, Hailiang, Li-Feng Cui, Yuan Yang, Hernan Sanchez Casalongue, Joshua Tucker Robinson, Yongye Liang, Yi Cui, and Hongjie Dai. “Mn_3O_4−Graphene Hybrid as a High-Capacity Anode Material for Lithium Ion Batteries.” Journal of the American Chemical Society 132, no. 40 (September 20, 2010): 13978–80.
47. Wu, Zhong-Shuai, Wencai Ren, Lei Wen, Libo Gao, Jinping Zhao, Zongping Chen, Guangmin Zhou, Feng Li, and Hui-Ming Cheng. “Graphene Anchored with Co_3O_4 Nanoparticles as Anode of Lithium Ion Batteries with Enhanced Reversible Capacity and Cyclic Performance.” *ACS Nano* 4, no. 6 (2010): 3187–94.
48. Luo, Zhiqiang, Luojia Liu, Jiaxin Ning, Kaixiang Lei, Yong Lu, Fujun Li, and Jun Chen. “A Microporous Covalent-Organic Framework with Abundant Accessible Carbonyl Groups for Lithium-Ion Batteries.” Angewandte Chemie International Edition 57, no. 30 (June 21, 2018): 9443–46.
49. Nitta, Naoki, Feixiang Wu, Jung Tae Lee, and Gleb Yushin. “Li-Ion Battery Materials: Present and Future.” *Materials Today* 18 no.5 (2015): 252–64.
50. Fan, Ling, Ruifang Ma, Jue Wang, Hongguan Yang, and Bingan Lu.“An Ultrafast and Highly Stable Potassium-Organic Battery.” *Advanced Materials* 30 no.51 (2018.): 1805486.
51. Raj, CR, and Sourav Mallick.“Aqueous Rechargeable Zn-Ion Battery: Strategies for Improving the Energy Storage Performance.” *ChemSusChem*, 2021.
52. Chao, Dongliang, Wanhai Zhou, Chao Ye, Qinghua Zhang, Yungui Chen, Lin Gu, Kenneth Davey, and Shi-Zhang Qiao. “An Electrolytic Zn–MnO_2 Battery for High-Voltage and Scalable Energy Storage.” *Angewandte Chemie* 131 no.23 (2019): 7905–10.

53. Zhao, Qing, Weiwei Huang, Zhiqiang Luo, Luojia Liu, Yong Lu, Yixin Li, Lin Li, Jinyan Hu, Hua Ma, and Jun Chen.“High-Capacity Aqueous Zinc Batteries Using Sustainable Quinone Electrodes.” *Science Advances* 4 no.3 (2018).
54. Bhanja, Piyali, Arindam Modak, and Asim Bhaumik.“Porous Organic Polymers for CO $_2$ Storage and Conversion Reactions.” *ChemCatChem* 11 no.1 (2018): 244–57.
55. Zhang, Ning, Xuyong Chen, Meng Yu, Zhiqiang Niu, Fangyi Cheng, and Jun Chen. “Materials Chemistry for Rechargeable Zinc-Ion Batteries.” *Chemical Society Reviews* 49 no.13 (2020): 4203–19.
56. Hu, Ping, Ting Zhu, Xuanpeng Wang, Xufeng Zhou, Xiujuan Wei, Xuhui Yao, Wen Luo, et al. “Aqueous Zn//Zn$(CF_3SO_3)_2$//$Na_3V_2(PO_4)_3$ Batteries with Simultaneous Zn^{2+}/Na^+ Intercalation/De-Intercalation.” *Nano Energy* 58 (2019): 492–98.
57. Chen, Xiudong, Hang Zhang, Yun Gao, Jin-Hang Liu, Xiaohua Cao, Changchao Zhan, Shitao Wang, Jiazhao Wang, Shi-Xue Dou, and Dapeng Cao. “Zinc-Ion Hybrid Supercapacitors: Design Strategies, Challenges, and Perspectives.” *Carbon Neutralization* 1 no.2 (2022): 159–88.
58. Zhang, Ning, Xuyong Chen, Meng Yu, Zhiqiang Niu, Fangyi Cheng, and Jun Chen. “Materials Chemistry for Rechargeable Zinc-Ion Batteries.” *Chemical Society Reviews* 49 no.13 (2020): 4203–19.
59. Khayum M, Abdul, Meena Ghosh, Vidyanand Vijayakumar, Arjun Halder, Maryam Nurhuda, Sushil Kumar, Matthew Addicoat, Sreekumar Kurungot, and Rahul Banerjee. “Zinc Ion Interactions in a Two-Dimensional Covalent Organic Framework Based Aqueous Zinc Ion Battery.” *Chemical Science* 10 no.38 (2019): 8889–94.
60. Krief, Pnina, James Y. Becker, Arkady Ellern, Vladimir Khodorkovsky, Ojars Neilands, and Lev Shapiro.“S-Indacene-1,3,5,7(2H,6H)-Tetraone (‘Janus Dione’) and 1,3-Dioxo-5,6-Indanedicarboxylic Acid: Old and New 1,3-Indandione Derivatives.” *ChemInform* 36 no. 9 (2005).
61. Wang, Wenjing, Mi Zhou, and Daqiang Yuan.“Carbon Dioxide Capture in Amorphous Porous Organic Polymers.” *Journal of Materials Chemistry A* 5 no.4 (2017): 1334–47.

APPENDICES

APPENDIX A:

^{1}H-NMR AND ^{13}C-NMR SPECTRA OF COMPOUND

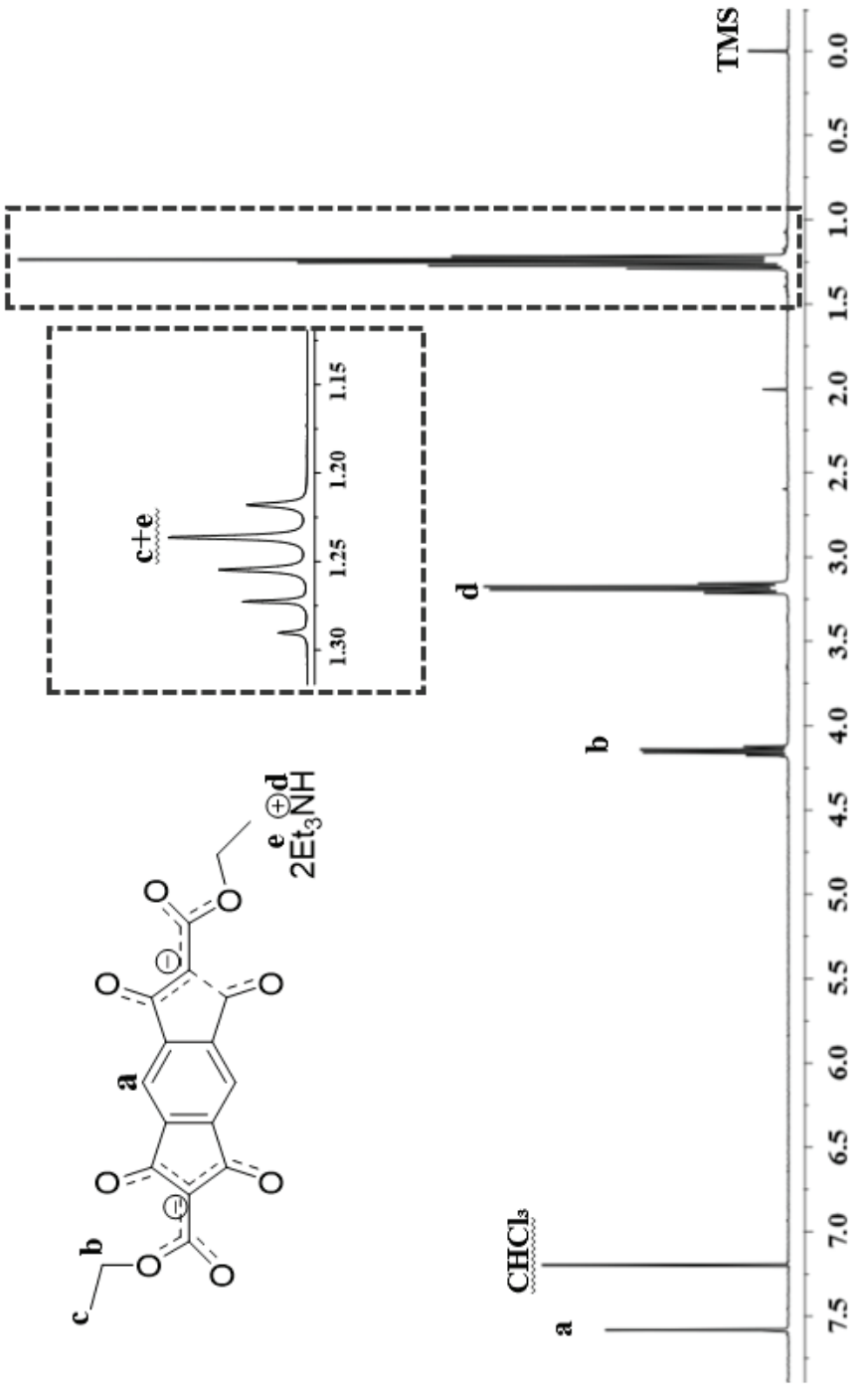

Figure 1. [1]H NMR of diethyl 1,3,5,7-tetraoxo-1,2,3,5,6,7-hexahydro-s-indacene-2,6-dicarboxylate(Compound)

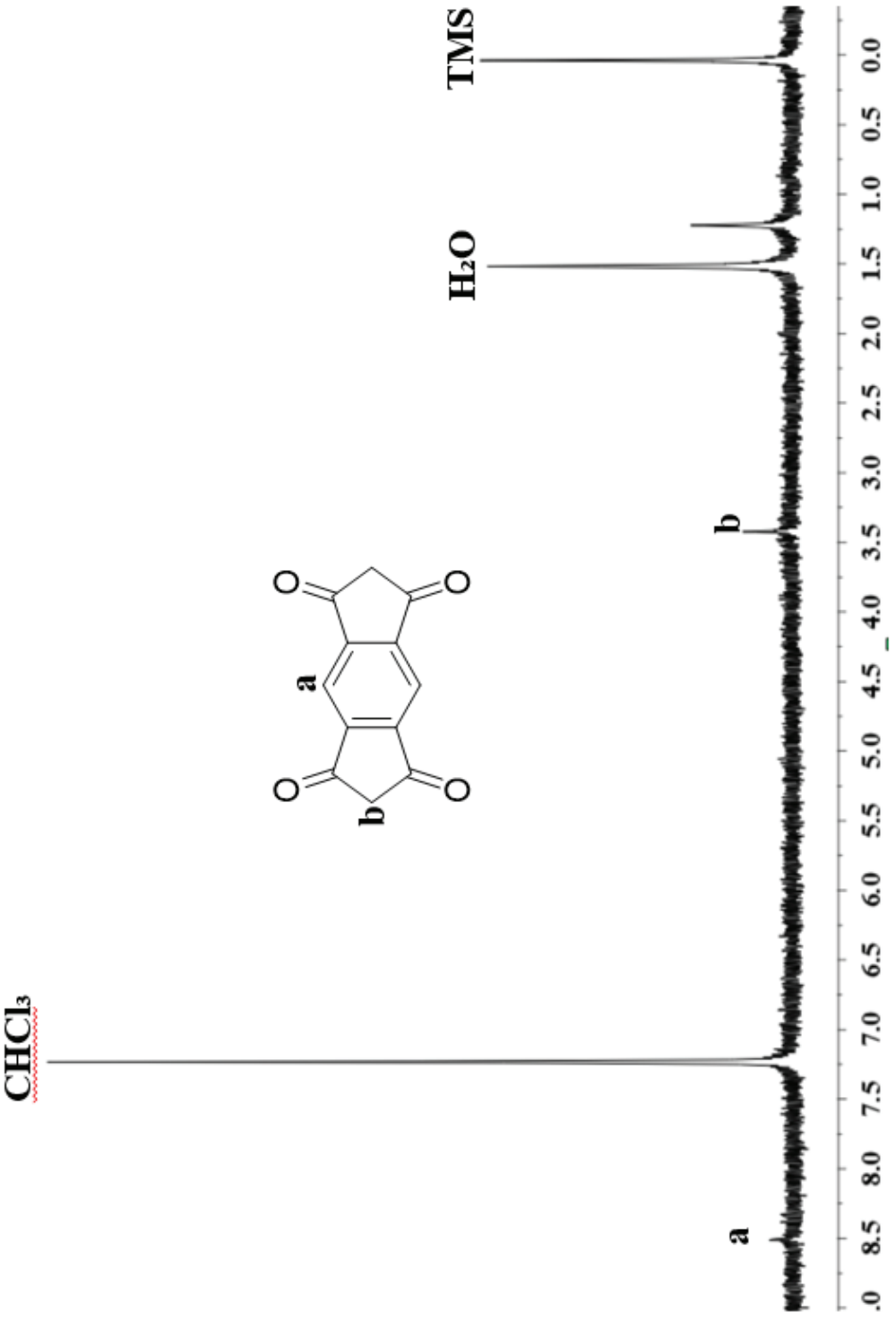

Figure 2. ^{1}H NMR of s-indacene-1,3,5,7(2H,6H)-tetraone (Monomer)

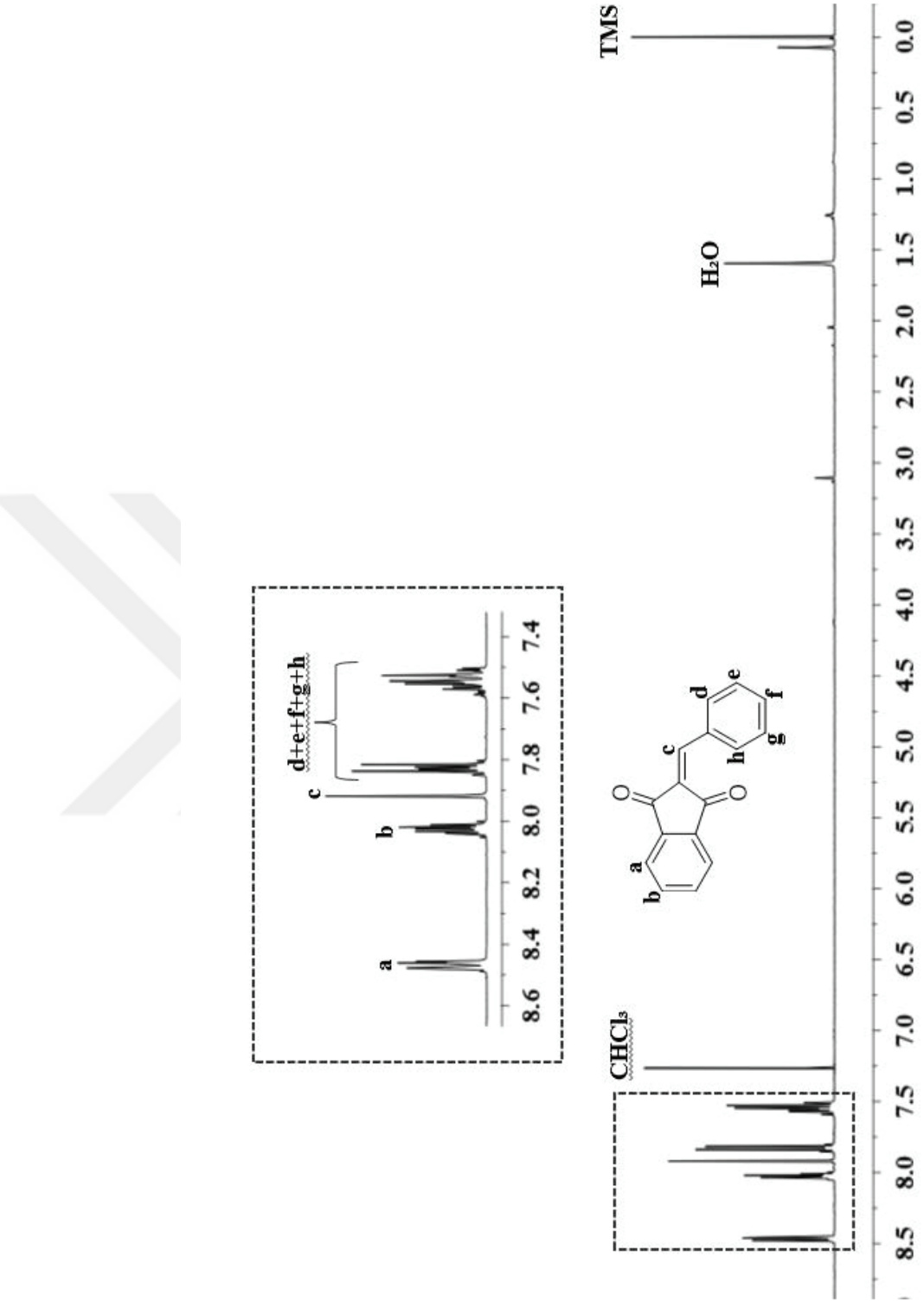

Figure 3. ^{1}H NMR of 2-benzylidene-1H-indene-1,3(2H)-dione (Model Compound)

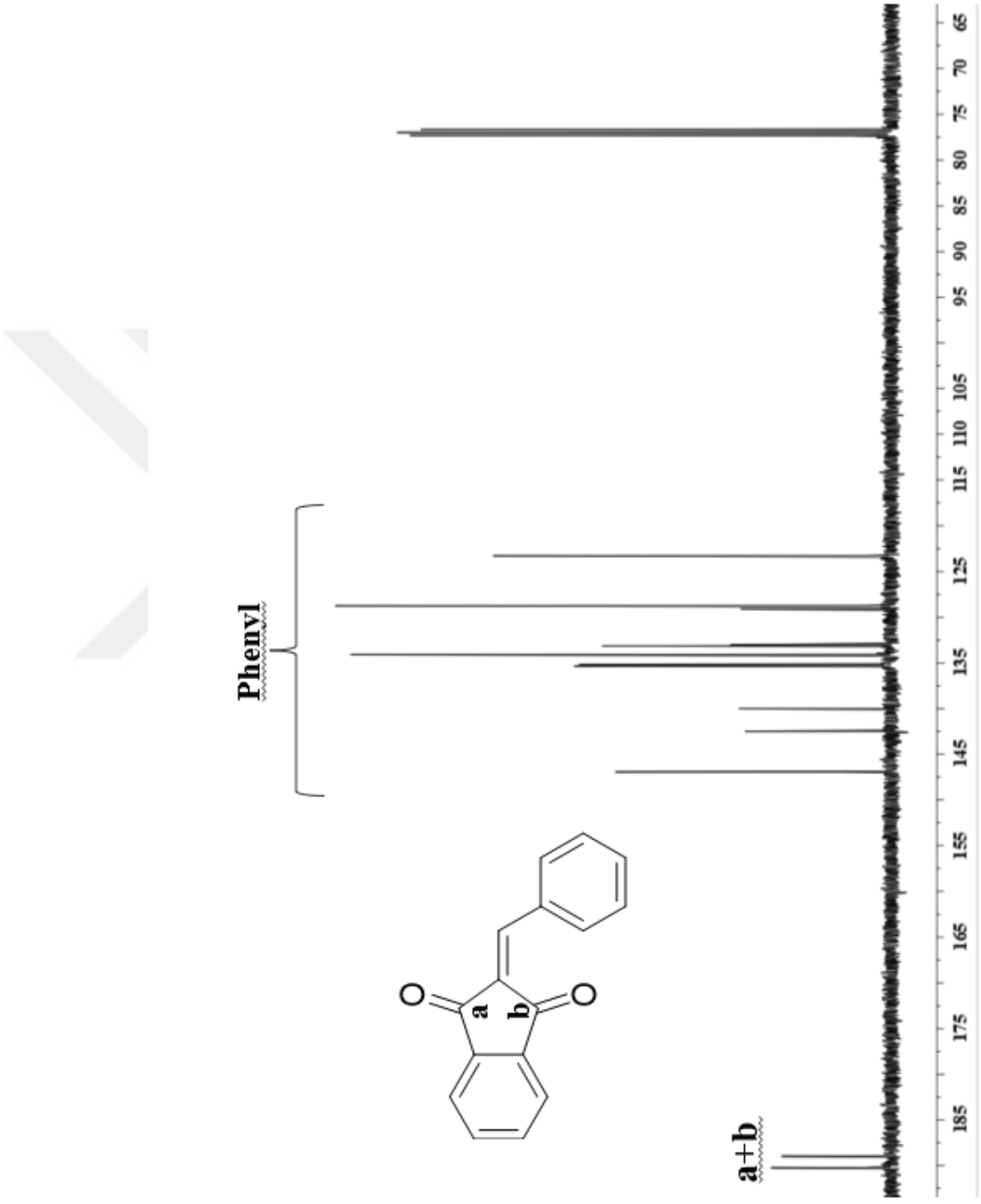

Figure 4. ^{13}C NMR of 2-benzylidene-1H-indene-1,3(2H)-dione (Model Compound)